Supporting Information

Ochiai et al. 10.1073/pnas.1202768109

SI Materials and Methods

Construction of Randomized Zinc-Finger Libraries and Bacterial One Hybrid (B1H) Selection. Construction of zinc-finger randomized libraries and B1H selection were carried out as described (1). To construct a series of reporter vectors for B1H selections, several sets of complementary oligonucleotide pairs corresponding to parts of the HpEts1 ZFN target sequence (Table S2) were synthesized, annealed, and inserted into the EcoRI/XmaI site of pH3U3-mcs (2).

Single-Strand Annealing (SSA) Assay. The SSA assay was carried out as described (1). To construct reporter vectors for the SSA assay, complementary oligonucleotides were annealed and inserted between the BsaI sites of the pGL4-SSA vector (Table S3) (1).

Construction of the Targeting Donor. A sea urchin genomic region spanning 2,410 bp (−1,137 to +1,273 nucleotides from the stop codon of the *HpEts1* gene) was amplified by PCR using Ets-HA-F and Ets-HA-R primers (Table S3) and subcloned into pBluescriptII SK(+) (Stratagene) to construct the pBSK-Ets-HA plasmid. Two oligonucleotides (2A-peptide-S and 2A-peptide-A) (Table S3) were synthesized and converted to double-stranded DNA by primer extension with KOD-plus- (TOYOBO). The 2A-peptide-encoding DNA fragment was subcloned into the EcoRV site of pBluescriptII SK(+), and a histone H2B (*H2B*)–*GFP* cassette (3) was cloned downstream of the 2A-peptide-encoding sequence to generate the pBSK-2A-H2B–GFP vector. The *2A-H2B–GFP* cassette was amplified by PCR with KOD-plus- using the 2A-peptide-2F and T3 promoter primers (Table S3). To generate the targeting donor construct pBSK-Ets-HRD, pBSK-Ets-HA was subjected to inverse PCR with the Ets-HA-inv-F and Ets-HA-inv-R primers (Table S3), followed by insertion of the amplified *2A-H2B–GFP* cassette. The Ets-HRD cassette was amplified by PCR with KOD-plus- using the Ets+T-F and Ets+T-R primers (Table S3) and pBSK-Ets-HRD as the template. To construct the targeting donor construct pBSK-Ets-HRD+T, which contains *HpEts1* ZFN target sites at both ends of the Ets-HRD cassette, the amplified Ets-HRD cassette was digested with XhoI and SpeI and inserted into the XhoI/SpeI sites of pBluescriptII SK(+).

Determination of the cDNA Sequence of HpLig4. A cDNA for the *Hemicentrotus pulcherrimus* homolog of DNA ligase IV (*HpLig4*) encoding the carboxyl-terminal tandem BRCT repeat (DN-lig4) was amplified by PCR from a cDNA library using primers for *HpLig4* (CTlig4F and CTlig4R) (Table S3). The amplified cDNA was subcloned into pBluescriptII SK(+), and the nucleotide sequence was determined by using a CEQ 8000 Genetic Analysis System (Beckman Coulter).

Sea Urchin Culture. Sea urchins (*H. pulcherrimus*) were harvested from the Seto Inland Sea or Tateyama Bay, Japan, and their gametes were obtained by coelomic injection of 0.55 M KCl. Fertilized eggs were cultured in filtered seawater at 16 °C.

mRNA Synthesis and Microinjection. A cDNA for B1H-SSA-selected ZFA was subcloned into transcription vectors containing a T7 promoter, the β-globin leader sequence, and either FokI nuclease domain variants *sharkey* RR (S418P, K441E, and D483R) or *sharkey* DS (S418P, K441E, E485A, and R489S) (4). The cDNA for DN-lig4 was subcloned into a transcription vector containing a T7 promoter and the β-globin leader sequence. The plasmids containing the *ZFN*, *DN-lig4*, or *ΔHpEts* (5) cDNAs were linearized with restriction enzymes. Polyadenylated *HpEts1 ZFN*, *DN-lig4*, and *ΔHpEts* mRNAs capped with an antireverse cap analog were synthesized by using a mMESSAGEmMACHINE T7 Ultra Kit (Ambion). The mRNAs were dissolved in 10% glycerol. Microinjection was conducted as described (6). Two picoliters of the solution containing targeting donor construct (20 fg/pl) with or without *ZFN* mRNAs (0.5 pg/pl each) and *DN-lig4* mRNA (2.5 pg/pl) was injected into each fertilized egg.

PCR-Based Genotyping Assay. Genomic DNA was isolated from ~300 control noninjected embryos and ~300 embryos injected with 1 pg of either of the *HpEts1 ZFN* mRNAs at 2.5 or 3.5 h postfertilization (hpf). A 357-bp PCR fragment containing the target sequence for the HpEts1 ZFNs was amplified by PCR using the Ets1F and Ets1R primers (Table S3). Aliquots (400 ng) of the PCR products were digested with AciI (New England Biolabs) overnight and analyzed by 3% agarose gel electrophoresis.

Western Blot Analysis. Embryos injected with 1 pg of *H2B–GFP* or *HpEts1–2A-H2B–GFP* mRNAs and noninjected control embryos at 20 hpf were sonicated in PBS for 30 s at 4 °C, dissolved in sample buffer (final concentrations: 0.35 M Tris-HCl, pH 6.8, 10.28% SDS, 36% glycerol, 5% β-mercaptoethanol, 0.012% bromophenol blue), and boiled for 5 min. Proteins were separated by using an electrophoresis device (ATTO) and then blotted to PVDF membranes (Millipore). For detection of GFP, the membranes were blocked with TBST [Tris-buffered saline containing 0.05% Tween 20, 5% (wt/vol) skim milk, 1.5% goat serum] and incubated with a purified polyclonal anti-GFP antibody (1:5,000; MBL) at 4 °C overnight. After washing with TBST, the membranes were incubated with HRP-conjugated anti-rabbit IgG (1:5,000; Pierce) for 1 h at room temperature. The chemiluminescence of Super Signal West Dura Extended Duration Substrate (Pierce) induced by hydrolysis with HRP was detected by X-ray film. Molecular weights were determined by using molecular weight standards (Precision Plus Protein Standards Dual Color; Bio-Rad).

Genomic PCR Analysis. Forty femtograms of the targeting donor construct alone or with 1 pg each of the *HpEts1 ZFN* mRNAs and/or 5 pg of *DN-lig4* mRNA was injected into fertilized sea urchin eggs. Genomic DNA was isolated from these embryos (~200 each) at 24 hpf by using a DNeasy Blood & Tissue Kit (Qiagen). The extracted genomic DNA was subjected to PCR by using KOD FX Neo (TOYOBO) with 0.3 μM gene-specific primers for *HpArs* (6) for 27 cycles (98 °C for 10 s, 60 °C for 30 s, and 68 °C for 1 min) or primers 1 and 2 (Table S3) for confirmation of targeted transgene insertion for 30 cycles (98 °C for 10 s and 68 °C for 1 min). The PCR products for *HpArs* and targeted transgene addition were separated in 2% and 1% agarose gels, respectively.

Live Imaging of Sea Urchin Embryos Using Epifluorescence Microscopy. Embryos were mounted in a microchamber assembled as follows: (*i*) high vacuum grease (Dow Corning) was applied at the corners of a 15-mm-wide square on a 35-mm glass-based dish (Iwaki); (*ii*) ~100 embryos were mouth-pipetted onto the center of the glass surface; (*iii*) the microchamber containing the embryos was closed with an 18 × 18-mm #1 coverslip (Matsunami); (*iv*) the corners of the coverslip were gently pressed to squeeze and immobilize the swimming embryos; and (*v*) the microchamber was filled with filtered seawater and sealed with mineral oil (Sigma-Aldrich). The embryos were visualized by using an IX-81 fluorescence microscope with a 60× 1.35-NA oil immersion objective (Olympus).

Live Imaging with Confocal Laser Scanning Microscopy (CLSM). Embryos injected with 40 fg of Ets-HRD+T donor vector, 1 pg of each *HpEts1 ZFN* mRNA, and 5 pg of *DN-lig4* mRNA with 1 pg of Texas Red-conjugated dextran (Invitrogen) for correction of the depth-dependent signal decay (7) were transferred into a microchamber as described above and visualized by using an FV1000-D CLSM with a 60× 1.2-NA water objective (Olympus). The same settings were used for all imaging experiments to simplify the comparison of the results. The pinhole was set to 304 μm, and the detector gain was set at 900 V for both Texas Red and GFP fluorescence. The same laser power (473-nm laser 25% power and 559-nm laser 60% power) was used for all measurements. Embryos were imaged at 2 μs per voxel in 2-μm-thick Z-sections for 30–40 slices. Fluorescence was recorded as an OIF file with an edge length of 256 pixels. To correct the depth-dependent signal decay, the confocal images for each embryo were processed by using ImageJ 1.44 software as described by Damle et al. (7) with some modifications (see below).

Imaging Data Analysis. CLSM offers the possibility of quantitative imaging of thin optical sections in living specimens. However, the quantification is confounded in thick samples, such as embryos, by optical distortion and internal light scattering. Although striking images can be collected by CLSM throughout an intact embryo, there is significant loss of signal at depths exceeding 10–15 μm. A simple depth correction is not adequate, because different tissue types have different optical properties that influence the severity of the signal loss. Recently, Damle et al. (7) described a method by which absolute numbers of GFP molecules could be deduced from CLSM image stacks in whole embryos of the sea urchin *Strongylocentrotus purpuratus*. To obtain an accurate measure of the depth-dependent loss of signal, a freely diffusible synthetic dye, Texas Red-labeled dextran, was injected into the eggs. The recovery of red fluorescence was then used to normalize the total fluorescence in deep optical sections to that in their shallower counterparts. We expected that application of this method to living *H2B–GFP* knock-in *H. pulcherrimus* embryos would enable us to quantify endogenous gene expression. To test this hypothesis, we injected *H2B–GFP* mRNA and Texas Red-conjugated dextran into eggs. Fluorescence images were then obtained by CLSM at 20 hpf. In contrast to the observations in *S. purpuratus*, the signal loss of Texas Red fluorescence was higher than that of GFP fluorescence in *H. pulcherrimus* (Fig. S5). However, we found that the mean relative fluorescence intensity of Texas Red raised to the power of 0.7 fit the mean relative fluorescence intensity of GFP well (Fig. S5). The confocal images for each embryo were recorded as OIF files and processed by using ImageJ software (8). Each image set comprised two image stacks: one measuring GFP fluorescence and the other measuring Texas Red fluorescence. Each image in a stack was square and contained 256 pixels. An image set was processed as follows. First, both GFP (473-nm excitation) and Texas Red (559-nm excitation) stack images were despeckled by using a 3 × 3 square median filter. Second, a Gaussian filter (1-pixel radius) was applied to each image within a stack. The threshold was set equal to the mean background fluorescence of each despeckled slice (200, 16-bit pixel units), and the average intensity above the background was calculated. An array of voxels with red intensity exceeding the threshold was created contiguous with the eight surrounding voxels (forming a 3 × 3 square) within the same horizontal plane, as described (9). The thresholded average intensity values for each slice in a stack were normalized to the highest value among those slices and raised to the power of 0.7. The coefficients of normalization constituted the depth profile for the stack. Third, a Gaussian filter was applied to the green stack, and the depth profile was used to compensate for the depth-dependent loss of GFP fluorescence. Fourth, the background fluorescence (250, 16-bit pixel units) was subtracted.

To quantify the mean fluorescence intensity of individual nuclei, processed images were analyzed as follows. First, a sequence of images containing nuclear fluorescence was extracted from a processed image stack and duplicated. Second, the duplicated stack was processed by a 3D hybrid median filter, Gaussian blur (sigma = 1), background subtraction (rolling ball radius = 30), and Z-projection (maximum intensity). In the obtained projection image, the center of each nucleus in which GFP fluorescence was detected above the background was manually selected with a 10-pixel-diameter circle, and the selected region of interest (ROI) was added to the ROI Manager. The selected ROIs were combined, the selection was inversed, and a mask was created. The mask was then divided by 255. To create an image stack in which the pixels outside the selected ROI had a zero value, all of the images in the untreated duplicate stack were multiplied by the processed mask. Third, the mean fluorescence intensity of each nucleus in the masked image stack was quantified by using a 3D object counter-tool (threshold = 200; filter size minimum = 30; "exclude objects on edges" was unchecked) (10).

1. Ochiai H, et al. (2010) Targeted mutagenesis in the sea urchin embryo using zinc-finger nucleases. *Genes Cells* 15:875–885.
2. Meng X, Noyes MB, Zhu LJ, Lawson ND, Wolfe SA (2008) Targeted gene inactivation in zebrafish using engineered zinc-finger nucleases. *Nat Biotechnol* 26: 695–701.
3. Fujii T, et al. (2009) Role of the nanos homolog during sea urchin development. *Dev Dyn* 238:2511–2521.
4. Guo J, Gaj T, Barbas, CF, 3rd (2010) Directed evolution of an enhanced and highly efficient FokI cleavage domain for zinc finger nucleases. *J Mol Biol* 400:96–107.
5. Kurokawa D, et al. (1999) HpEts, an ets-related transcription factor implicated in primary mesenchyme cell differentiation in the sea urchin embryo. *Mech Dev* 80: 41–52.
6. Ochiai H, Sakamoto N, Momiyama A, Akasaka K, Yamamoto T (2008) Analysis of cis-regulatory elements controlling spatio-temporal expression of T-brain gene in sea urchin, Hemicentrotus pulcherrimus. *Mech Dev* 125:2–17.
7. Damle S, Hanser B, Davidson EH, Fraser SE (2006) Confocal quantification of cis-regulatory reporter gene expression in living sea urchin. *Dev Biol* 299:543–550.
8. Abràmoff MD, Magalhaes PJ, Ram SJ (2004) Image processing with ImageJ. *Biophoton Int* 11:36–42.
9. Dmochowski IJ, Dmochowski JE, Oliveri P, Davidson EH, Fraser SE (2002) Quantitative imaging of cis-regulatory reporters in living embryos. *Proc Natl Acad Sci USA* 99: 12895–12900.
10. Bolte S, Cordelières FP (2006) A guided tour into subcellular colocalization analysis in light microscopy. *J Microsc* 224:213–232.

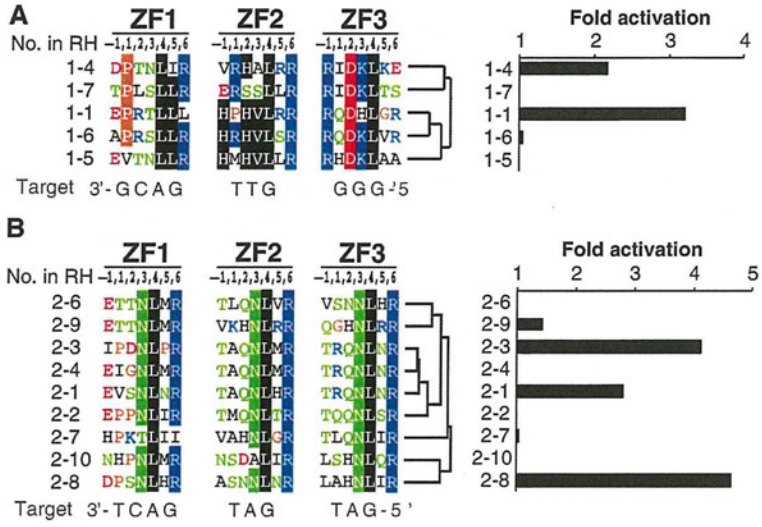

Fig. S1. Alignment of the predicted amino acid sequences of the recognition helices in the selected ZF arrays. The predicted amino acid sequences of the recognition helices (residues −1 to +6) in the ZF arrays selected by the B1H system are aligned in *A Left* and *B Left*. The alignments shown in *A* and *B* were derived from selected clones for the HpEts1L (5′-GGGGTTGACG-3′) and HpEts1R (5′-GATGATGACT-3′) target sites, respectively. Residues present in more than three (*A*) or five (*B*) of the clones are highlighted. The numbers of residues in the recognition helix (represented as No. in RH) and the target sequences are shown above and below each alignment, respectively. The phylogenetic trees are shown in *A Center* and *B Center*. The cellular activities of the engineered ZFNs as homodimers are shown in *A Right* and *B Right*. The fold activation of recombination by each ZFN represents the luciferase expression level in cells cotransfected with the ZFN vector, SSA reporter vector, and pRL-CMV reference vector compared with that in cells transfected with a control empty vector, SSA reporter vector, and reference vector. In this study, we used the 1-1 and 2-8 ZFNs as HpEts1L and HpEts1R ZFNs, respectively.

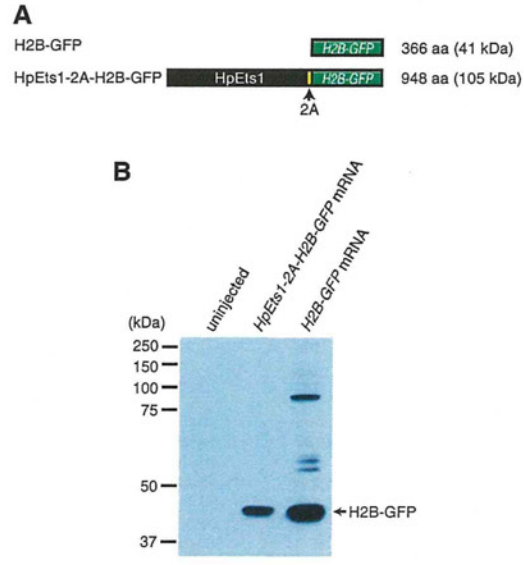

Fig. S2. 2A peptide mediates protein cleavage in sea urchin embryos. To verify that the 2A-linked proteins were cleaved efficiently in sea urchin embryos, we injected *H2B–GFP* and *HpEts1–2A-H2B–GFP* mRNAs, in which HpEts1 and H2B–GFP were linked with 2A peptide, and performed a Western blot analysis. (*A*) Structures of the constructs used in this study. (*B*) Western blot analysis with an anti-GFP antibody. In the *HpEts1–2A-H2B–GFP* mRNA-injected embryos, only one signal with a similar electrophoretic mobility to that of H2B–GFP was detected, suggesting that 2A-linked proteins were cleaved efficiently in sea urchin embryos.

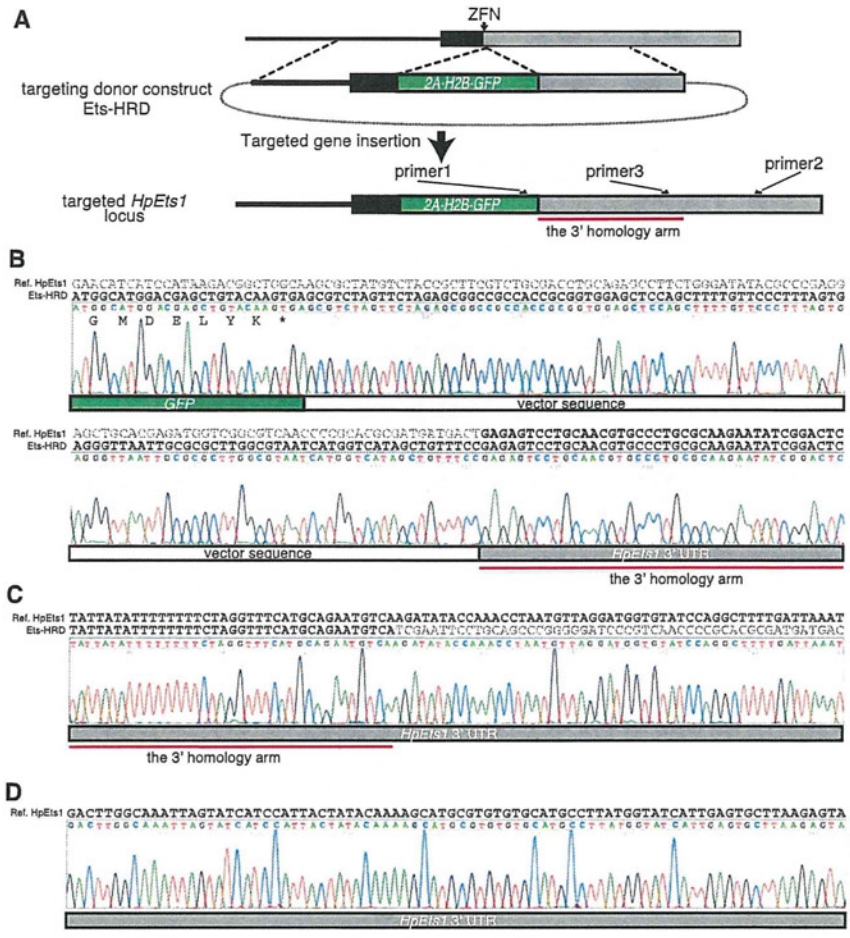

Fig. S3. Sequence analysis for confirmation of the occurrence of targeted transgene insertion. As shown in Fig. 2*C*, ZFN-mediated targeted gene insertion was confirmed by genomic PCR using primers 1 and 2. To verify the fidelity of the PCR amplification, the PCR products were cloned and sequenced. (*A*) Targeting donor construct (Ets-HRD or Ets-HRD+T; latter vector was omitted for clarity) for insertion of a *2A-H2B–GFP* cassette into the *HpEts1* locus. The structure of the *HpEts1* exon 8 and the targeted *HpEts1* allele are shown in *Lower*. The gray and black boxes represent coding and noncoding exons, respectively. The red bar represents the 3′ homology arm region. The primer sites for the genomic PCR and sequencing analysis are indicated. (*B–D*) Representative sequence data of the PCR products derived from ZFN/Ets-HRD-coinjected embryos using primer 1 (*B*), primer 3 (*C*), and primer 2 (*D*). The corresponding HpEts1 genomic sequence and Ets-HRD targeting donor vector sequence are shown above each set of sequence data. We obtained the same results by using PCR products derived from embryos coinjected with ZFN/Ets-HRD+T or ZFN/Ets-HRD+T/DN-lig4.

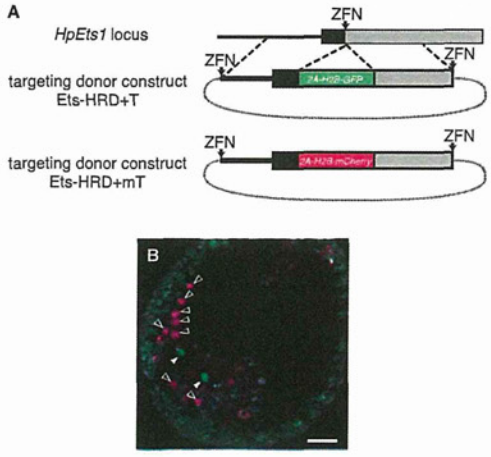

Fig. S4. Cointroduction of Ets-HRD+T and Ets-HRD+mT targeting donor constructs. (*A*) Structures of the targeting donor constructs Ets-HRD+T and Ets-HRD +mT, comprising the Ets-HRD+T cassette with *mCherry* instead of *GFP*. (*B*) Projection of the z-stack images of an embryo with GFP-expressing primary mesenchyme cells (PMCs) and mCherry-expressing PMCs. A fluorescence image of an embryo coinjected with *HpEts1 ZFNs*, *DN-lig4* mRNAs, Ets-HRD+T, and Ets-HRD +mT was obtained at 24 hpf using CLSM. The filled and open arrowheads indicate GFP-expressing (green) and mCherry-expressing (purple) PMCs, respectively. (Scale bar, 20 μm.)

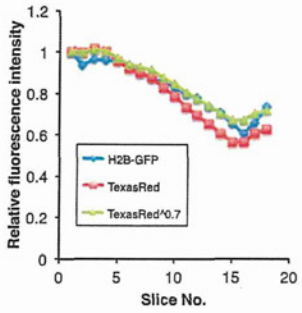

Fig. S5. Depth profiles of GFP and Texas Red in sea urchin embryos at 20 hpf. The overlaid plots of the mean intensity (minus threshold) vs. the number of slices (depth) for GFP and Texas Red are slightly different. The values representing the mean relative fluorescence intensity of Texas Red raised to the power of 0.7 are well fitted to the values of the mean relative fluorescence intensity of GFP.

Table S1. Numbers of GFP-positive PMCs observed in individual embryos

	No. of GFP-positive PMCs observed in each embryo			
Embryo ID	Count	Count	Count	Count
1*	43*			
2*	43*			
3*	40*			
4*	39*			
5*	36*			
6*	34*			
7*	32*			
8*	31*			
9*	31*			
10*	29*			
11*	27*			
12*	27*			
13*	23*			
14		16		
15		15		
16		15		
17		14		
18		10		
19			8	
20			8	
21			8	
22			5	
23			5	
24			5	
25			5	
26			5	
27			5	
28			5	
29				4
30				4
31				3
Average	33	12	6	4
Developmental stage when targeted insertion occurs	2-cell	4-, 8-, 16-, and 32-cell	60-cell	Molura or later
No. of PMC-generating cells at stage	2	4	8	16 or more
Theoretical no. of GFP-positive PMCs	$(55 \pm 10^{\dagger})/2$	$(55 \pm 10^{\dagger})/4$	$(55 \pm 10^{\dagger})/8$	$(55 \pm 10^{\dagger})/16$

*The embryos have still GFP-negative PMCs, suggesting that the targeted insertion occurs at least after the first division.
†In *H. pulcherrimus*, it has been reported that there are 55 ± 10 PMCs at the gastrula stage (see ref. 1).

1. Kominami T, Takaichi M (1998) Unequal divisions at the third cleavage increase the number of primary mesenchyme cells in sea urchin embryos. *Dev Growth Differ* 40:545–553.

Table S2. Nucleotide sequences of oligonucleotides used for preparation of pH3U3-B1H-reporter vectors

ZFN target site	HpEts target subsite	Oligonucleotides		Nucleotide sequence
HpEts1	Subsite for ZF1, ZF2 and ZF3	B1HT- Ets1S	Sense	5′-CCGGCGGGGTTGACGTGTC-3′
		B1HT-Ets1A	Antisense	5′-AATTGACACGTCAACCCCG-3′
	Subsite for ZF3	B1HT-Ets1-3S	Sense	5′-CCGGCGGGGATGGTGTGTC-3′
		B1HT-Ets1-3A	Antisense	5′-AATTGACACACCATCCCCG-3′
	Subsite for ZF2	B1HT-Ets1-2S	Sense	5′-CCGGCGAAGTTGGTGTGTC-3′
		B1HT-Ets1-2A	Antisense	5-AATTGACACACCAACTTCG-3′
	Subsite for ZF1	B1HT-Ets1-1S	Sense	5′-CCGGCGAAGATGACGTGTC-3′
		B1HT-Ets1-1A	Antisense	5′-AATTGACACGTCATCTTCG-3′
HpEts 2	Subsite for ZF1, ZF2 and ZF3	B1HT-Ets2S	Sense	5′-CCGGCGATGATGACTTGTC-3′
		B1HT-Ets2A	Antisense	5′-AATTGACAAGTCATCATCG-3′
	Subsite for ZF3	B1HT-Ets2-3S	Sense	5′-CCGGCGATGATGGTTTGTC-3′
		B1HT-Ets2-3A	Antisense	5′-AATTGACAAACCATCATCG-3′
	Subsite for ZF2	B1HT-Ets2-2S	Sense	5′-CCGGCGAAGATGGTTTGTC-3′
		B1HT-Ets2-2A	Antisense	5′-AATTGACAAACCATCTTCG-3′
	Subsite for ZF1	B1HT-Ets2-1S	Sense	5′-CCGGCGAAGATGACTTGTC-3′
		B1HT-Ets2-1A	Antisense	5′-AATTGACAAGTCATCTTCG-3′

Table S3. Names and nucleotide sequences of oligonucleotides used in this study

Oligonucleotides	Nucleotide sequences (5′ -> 3′)
SSA-GL4-Ets1-S	GTCGGACGTCAACCCCGTGACCGGGGTTGACGGGT
SSA-GL4-Ets1-A	CGGTACCCGTCAACCCCGGTCACGGGGTTGACGTC
SSA-GL4-Ets2-S	GTCGGAAGTCATCATCGGTGTCGATGATGACTGGT
SSA-GL4-Ets2-A	CGGTACCAGTCATCATCGACACCGATGATGACTTC
Ets-HA-F	ATTACTGGCAGTGGTAACAG
Ets-HA-R	GACATTCTGCATGAAACCTAG
2A peptide-S	GAAGATCTTGCTGCCTCGAGGAGGGAAGAGGTAGCCTGCTAACTTGCGG
2A peptide-R	GCTCTAGAGGGACCAGGATTTTCCTCTACGTCCCCGCAAGTTAGCAGGC
2A peptide-2F	GAGGGAAGAGGTAGCCTGCT
T3 promoter primer	ATTAACCCTCACTAAAGGGA
Ets HA-inv-F	TGAGAGTCCTGCAACGTGCC
Ets HA-inv-R	ATCGTCGTCGCGTGCTGGAT
Ets+T-F	GGCCCCCCCTCGAGCGTCAACCCCGCACGCGATGATGACTGTCGACGGTATCGATAAGCTTGATA
Ets+T-R	GCTCTAGAACTAGTAGTCATCATCGCGTGCGGGGTTGACGGGATCCCCCGGGCTGCAGGAATTCG
Ets1F	ACCCAAGATGAACTACCCGAAGC
Ets1R	GGAAAAAGCGACACTCCTCC
primer1	GCATCAAGGTCAACTTCAAGATCAGA
primer2	TGGCAAGTTTGGACAAAATTACATTC
CTlig4F	CTGAATTCCTGGAGGGACGAGAGCTCTGTATCATG
CTlig4R	CTCTCGAGTCAAGACATTGCTGCTTCRTA*

*R = A or G.

nature COMMUNICATIONS

OPEN

ARTICLE

Received 6 Jun 2012 | Accepted 24 Jul 2012 | Published 21 Aug 2012

DOI: 10.1038/ncomms2020

Non-transgenic genome modifications in a hemimetabolous insect using zinc-finger and TAL effector nucleases

Takahito Watanabe[1], Hiroshi Ochiai[2], Tetsushi Sakuma[2], Hadley W. Horch[3], Naoya Hamaguchi[1], Taro Nakamura[1], Tetsuya Bando[1], Hideyo Ohuchi[1], Takashi Yamamoto[2], Sumihare Noji[1] & Taro Mito[1]

Hemimetabolous, or incompletely metamorphosing, insects are phylogenetically relatively basal and comprise many pests. However, the absence of a sophisticated genetic model system, or targeted gene-manipulation system, has limited research on hemimetabolous species. Here we use zinc-finger nuclease and transcription activator-like effector nuclease technologies to produce genetic knockouts in the hemimetabolous insect *Gryllus bimaculatus*. Following the microinjection of mRNAs encoding zinc-finger nucleases or transcription activator-like effector nucleases into cricket embryos, targeting of a transgene or endogenous gene results in sequence-specific mutations. Up to 48% of founder animals transmit disrupted gene alleles after zinc-finger nucleases microinjection compared with 17% after microinjection of transcription activator-like effector nucleases. Heterozygous offspring is selected using mutation detection assays that use a Surveyor (Cel-I) nuclease, and subsequent sibling crosses create homozygous knockout crickets. This approach is independent from a mutant phenotype or the genetic tractability of the organism of interest and can potentially be applied to manage insect pests using a non-transgenic strategy.

[1] Department of Life Systems, Institute of Technology and Science, University of Tokushima, 2-1 Minami-Jyosanjima-cho, Tokushima 770-8506, Japan. [2] Department of Mathematical and Life Sciences, Graduate School of Science, Hiroshima University, 1-3-1 Kagamiyama, Higashi-Hiroshima 739-8526, Japan. [3] Department of Biology and Neuroscience, Bowdoin College, Brunswick, Maine 04011, USA. Correspondence and requests for materials should be addressed to T.M. (email: mito@bio.tokushima-u.ac.jp).

Continuous improvements in DNA sequencing technologies continue to facilitate sequence analyses of complete genomes of numerous species. Moreover, the ability to directly and specifically manipulate a genome, for example, by generating specific gene knockouts, is essential for elucidating gene function on a genome-wide scale. However, the molecular tools and methods needed for gene targeting require a functional genomics approach. Thus, these techniques have been limited to the study of certain well-established model organisms, including yeast[1], fruitflies[2] and mice[3], although approaches in these systems are still often inefficient. As a result, a systematic, reverse genetic analysis of crickets, and perhaps other lesser-studied species, has been limited by the absence of a suitable genome-manipulation technique, until now.

Engineered nucleases, including zinc-finger nucleases (ZFNs) and transcription activator-like effector nucleases (TALENs), are powerful tools for genome editing based on their capacity to target a specific genomic locus[4,5]. For example, ZFNs can be generated by linking the nonspecific cleavage domain of the *Fok*I restriction endonuclease to a DNA-binding domain composed of modular zinc-finger (ZF) domains[4]. Each ZF domain primarily contacts three base pairs (bps) within the major groove of DNA. However, ZFs can be modified to recognize a broad range of DNA sequences[4,6]. Ideally, a pair of ZFNs is designed for a particular target, whereby dimerization of the associated cleavage domains is accommodated and a double-stranded break (DSB) is introduced (Fig. 1a)[6,7]. Alternatively, TALENs consist of an engineered array of TAL effector repeats fused to the *Fok*I cleavage domain, and can also introduce targeted DSBs in DNA[5]. The DNA-binding domains of TALEs have tandem repeat units (each 33–35 aa in length), in which the nucleotide binding preference is determined by the two adjacent amino acids, and these are referred to as the repeat variable di-residue[8]. For both systems, DSBs can be restored via cellular DNA repair pathways, which include non-homologous end-joining (NHEJ) mechanisms and homologous recombination mechanisms. For NHEJ-based repairs of ZFN/TALEN-induced DSBs, small insertions and/or deletions (indels) are produced at the repair junction, thereby generating mutations precisely at the cleavage site (Fig. 1a)[9].

ZFN-targeted mutations have been induced in several organisms, including fruitflies[10–12], silkworms[13], zebrafish[14], rats[15,16], sea urchins[17], roundworms[18], frogs[19] and mice[20,21]. More recently, TALENs have been applied to rats[22], zebrafish[23] and fruitflies[24]. In both models, mRNA was directly injected into embryos. However, the success of this method in engineering homozygous knockout animals that exhibit null phenotypes has had limited success, and has only been reported in fruitflies[10,24], zebrafish[14,23] and rats[15,16,22]. In these cases, selective breeding with animals that bear specific genetic markers, or morphologically detectable phenotypes, was performed after ZFN mutagenesis. Correspondingly, these approaches depended on genetic tractability, or the characteristics of the phenotypes generated. To facilitate a more generally applicable knockout analysis in various organisms, including non-model ones, a strategy to apply ZFN/TALEN-mediated mutagenesis for the generation of homozygous knockout animals was investigated.

The cricket, *Gryllus bimaculatus* (Orthoptera), is an emerging model system that has been used to study developmental biology and mechanisms of regeneration based on the success of RNA interference (RNAi)-based gene-functional analyses and transgenic technology in this system[25,26]. It is possible that this cricket model could also be used to characterize the molecular mechanisms relevant to human diseases, and be a model for the screening of therapeutic drugs with RNAi[27]. However, while the cricket is currently used as a model system in the fields of neuroethology, endocrinology and behavioural ecology, the introduction of targeted and heritable mutations has remained intractable in this species. Therefore, the ability to edit the cricket genome would further enhance studies performed in all of these fields.

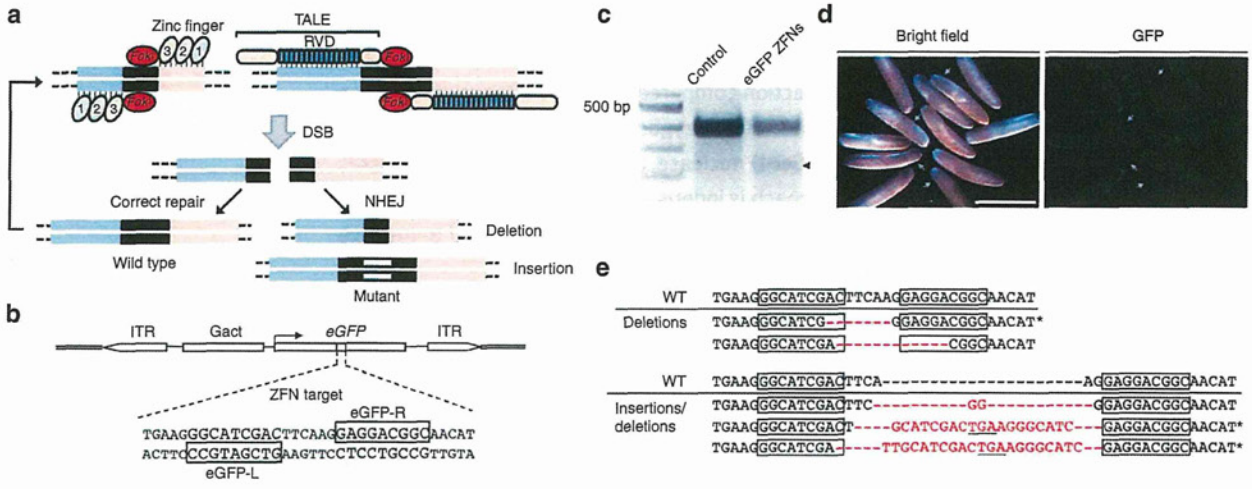

Figure 1 | Disruption of an *eGFP* transgene in *G. bimaculatus* using designed ZFNs. (**a**) Illustration of the binding and function of ZFNs and TALENs. Following the introduction of double-stranded breaks (DSB) in the DNA between targeted binding sites, these breaks are either repaired and digested again, or NHEJ can occur and deletions or insertions can result. In the latter case, gene function of the targeted gene is disrupted, and subsequent binding of ZFNs or TALENs does not result in *Fok*I dimerization or the generation of DSBs. (**b**) Structure of the pBGact-*eGFP* transgene that is under the transcriptional control of the *Gryllus* cytoplasmic *actin* promoter (Gact) and flanked by 5′ and 3′ inverted terminal repeats (ITRs). The 9-bp binding sites for the ZFNs, eGFP-R and eGFP-L are in the boxes shown. (**c**) Detection of induced mutations into genomic DNA cleaved by Surveyor nuclease that was collected from embryos injected with both eGFP-R and eGFP-L mRNAs or eGFP-R mRNA alone (control) at 7 days postinjection. A product cleaved by Surveyor nuclease was detected in the genomic DNA from embryos injected with eGFP-R/L mRNAs (arrowhead). (**d**) Bright field (left panel) and fluorescence (right panel) phenotypes of G_1 crickets injected with *eGFP* ZFN mRNA at 2 days after egg laying. While the embryos appeared to develop normally, some embryos did not exhibit *eGFP* fluorescence (indicated with arrows). Scale bar, 2.5 mm. (**e**) Sequence analysis of *eGFP* mutant alleles induced by *eGFP* ZFN mRNAs. Wild-type (WT) sequences are shown above the mutant sequences containing deletions (indicated with dashes) and/or insertions (shown in red letters). Asterisks indicate knockout mutations that included frame-shift and stop codon insertions (underlined).

Here we report the generation of homozygous knockouts of an endogenous gene in *G. bimaculatus* via ZFN- and TALEN-based targeted mutagenesis. A simple, efficient and broadly applicable approach is described for the construction of gene knockouts, and this approach involves the direct injection of mRNAs encoding ZFNs or TALENs into embryos, combined with mutant detection assays that use the Surveyor (Cel-I) nuclease.

Results

Testing the functionality of ZFNs in cricket embryos. As proof of principle, the function of ZFNs targeted to an *eGFP* (*enhanced green fluorescent protein*) transgene in the cricket genome was evaluated. Specifically, two ZFNs, eGFP-L and eGFP-R, were designed to target the coding region of the *eGFP* gene (Fig. 1b; Table 1). To generate these functional ZFNs, a bacterial one-hybrid (B1H) system using randomized libraries of ZF domains and single-strand annealing (SSA) assays performed in cultured cells were used[17,28]. The ZF proteins assembled were linked to variants of the *Fok*I nuclease domain. These variants functioned as obligate heterodimers to reduce their propensity for homodimerization, thereby decreasing the frequency of off-target cleavage events[29]. Coinjections of mRNAs of eGFP-L and eGFP-R into heterozygous *eGFP* transgenic cricket eggs were then performed[26]. As negative controls, eGFP-L or eGFP-R mRNAs were injected individually. After 7 days, genomic DNA was extracted from ZFN-treated and control embryos in the G_0 generation, and the mismatch-sensitive endonuclease, Surveyor (Cel-I)[30], was used to screen these DNA samples. The results of these assays demonstrated that mutations were induced in the targeted locus of ZFN-treated embryos, yet not in the controls (Fig. 1c). Moreover, fluorescence was detected in the G_1 generation of transgenic cricket embryos carrying *eGFP* in the control group (untreated), and not in a subset of ZFN-treated embryos (Fig. 1d; Table 2). Subsequent sequence analyses of targeted loci in the G_1 embryos revealed that the ZFN-induced mutations contained multiple indels ranging from 4 to 28 bp centred over the ZFN recognition site (Fig. 1e). These results indicate that the mutations present resulted from NHEJ. Thus, a lack of *eGFP*-encoded fluorescence and mutations of the wild-type *eGFP* DNA sequence indicated that knockout of the *eGFP* transgene had been achieved. In combination, these results show that engineered ZFNs can induce mutations in a targeted locus of the cricket genome, and this DSB induces error-prone NHEJ repair.

Mutagenesis of an endogenous gene with ZFNs. To evaluate the capacity for a ZFN to produce a knockout model, disruption of the endogenous phenoloxidase gene *G. bimaculatus laccase2* (*Gb'lac2*) was targeted. This gene was selected based on previous studies in which RNAi targeting of *Gb'lac2* in the nymphal stages of the cricket resulted in loss of cuticle tanning after molting[25].

An open reading frame sequence appropriate for the assembly of ZFNs was identified in the second oxidase domains of the *Gb'lac2* gene (Fig. 2a; Table 1). To achieve a high efficiency of mutagenesis, derivatives of the *Sharkey* cleavage domain were used for the assembly of ZFNs[31]. The mRNA of assembled ZFNs was then injected into cricket eggs. After 2 days, morphological defects were observed. All embryos injected with 1 $\mu g\,\mu l^{-1}$ *Gb'lac2* ZFN mRNA died, or exhibited abnormal development (Fig. 2b). Furthermore, when ZFN mRNAs were administered at lower concentrations, abnormal development was reduced, and 2 days after injection, embryos were comparable to normal control embryos (for example, embryos only injected with Lac2-L; Fig. 2b). The Surveyor nuclease assay was able to detect the ZFN-induced mutations in embryos injected with each *Gb'lac2* ZFN mRNA at the reduced concentration of 1 $ng\,\mu l^{-1}$, at least (Fig. 2c). Hatched nymphs were also reared from embryos injected with 1 $ng\,\mu l^{-1}$ mRNAs, and ~58% of the fifth-instar G_0 larvae of this group exhibited a mosaic cuticle pattern with and without tanning (Fig. 2d; Table 2). Therefore, the presence of somatic mutants was confirmed.

Generation of homozygous knockout crickets. To generate a homozygous knockout of *Gb'lac2*, a simple genetic scheme was designed where mates with a specialized genetic background were not needed (Fig. 3a). As the first step, ZFN-treated G_0 crickets (with

Table 1 | *eGFP* and *Gb'lac2* ZFNs target sites and amino-acid sequences of designed ZF recognition helices.

ZFN	ZFN binding sequence	Finger 1	Finger 2	Finger 3
eGFP-R	5′-GGCATCGACttcaagGAGGACGGC-3′	TSGHLVR	DLANLNR	RPDNLAH
eGFP-L	5′-CCGTAGCTGaagttcCTCCTGCCG-3′	RQRELLR	VTHNLTR	DQSALVR
Lac2-R	5′-CCTGACGACgcacgtGATGCTGCT-3′	RSHDLLR	TTTDLRR	RRHHLQH
Lac2-L	5′-GGACTGCTGcgtgcaCTACGACGA-3′	RKMHLTV	DSSSLIR	DASALRR

Each ZFNs target sites are indicated by the underlines. Fingers 1–3 show the amino acids of zinc-finger recognition helices of each ZFNs.

Table 2 | ZFN- or TALEN-induced mutagenesis after mRNA microinjection in insects.

ZFNs/TALENs	Number of injected eggs	Somatic mutants, *n* (Mut/G0 nymph, %)	Fertile adults, *n* (adults/injected eggs, %)	Germline mutants, *n* (Mut/crossed adults*, %)	Reference
Gb eGFP-ZFN-L, R	302	ND	64 (22)	10 (48)	This study
Gb eGFP-ZFN-L or R	74	ND	14 (19)	0	This study
Gb Lac2- ZFN-L, R	358	54 (58)	32 (7)	15 (47)	This study
Gb Lac2- ZFN-L or R	84	0	7 (8)	0	This study
Gb Lac2- TALEN-L, R	168	18 (17)	35 (21)	6 (17)	This study
Gb Lac2- TALEN-L or R	62	0	11 (18)	0	This study
Bm BL-1 (ZFN)*	480	ND (72)	173 (36)	5-9 (9-16)	Ref. 13
Dm rosy (ZFN)	ND	ND	99 (4-30)	41 (41)	Ref. 11
Dm yellow (TALEN)	ND	32 (44)	109 (ND)	33 (31)	Ref. 24

Abbreviations: *Bm, Bombyx mori; Dm, Drosophila melanogaster; Gb, Gryllus bimaculatus;* ND, not determined.
*In the *Bombyx* studies, males were crossed.

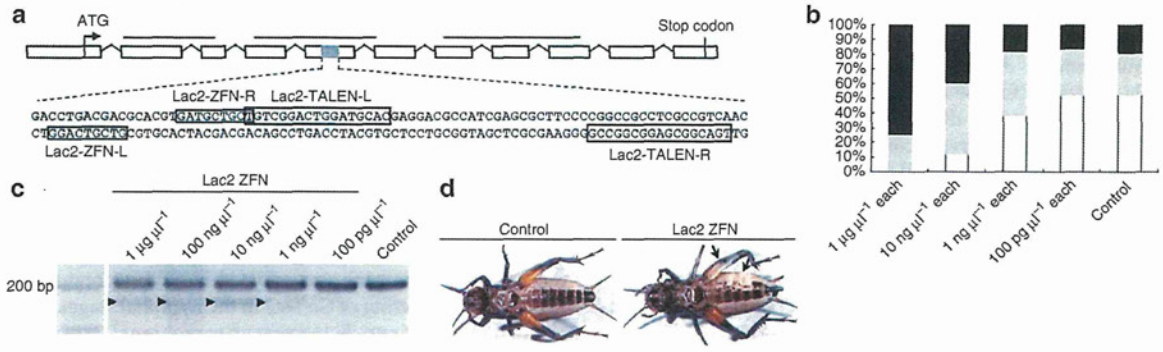

Figure 2 | Design and application of ZFNs and TALENs targeted to *Gb'lac2*. (**a**) Structure of the *Gb'lac2* gene, with open boxes representing exons mapped on the *Gryllus* genomic sequence. Black bars indicate Cu-oxidase domains 1–3. The grey region of the fifth exon is expanded to provide the gene sequence that includes the 9 or 17 bp ZFN and TALEN binding sites, respectively (shown in boxes). (**b**) Dose-dependent toxicity of *Gb'lac2* ZFN mRNAs in cricket embryos. The percentages of dead (black), deformed (grey) and normal (white) embryos at 2 days postinjection are shown. The control was embryos injected with Lac2-L ZFN mRNA alone. The percentage of embryos that developed normally increased with decreasing concentrations of *Gb'lac2* ZFN mRNAs (0/43 for 1 $\mu g\,\mu l^{-1}$ each, 6/51 for 10 $ng\,\mu l^{-1}$ each, 19/50 for 1 $ng\,\mu l^{-1}$ each, 13/25 for 100 $pg\,\mu l^{-1}$ each and 11/21 for control). (**c**) Using a Surveyor nuclease assay, mutations in *Gb'lac2* were detected following the microinjection of crickets with *Gb'lac2* ZFN mRNAs. Products cleaved by Surveyor nuclease (indicated with arrowheads) were detected at 1 $\mu g\,\mu l^{-1}$, 100 $ng\,\mu l^{-1}$, 10 $ng\,\mu l^{-1}$ and 1 $ng\,\mu l^{-1}$ of Lac2 ZFN injected. (**d**) Imaging of control and *Gb'lac2* ZFN final-instar nymphs. Mutagenesis of somatic cells in G_0 crickets was detected based on the presence of a white spot phenotype by epidermal cells (indicated with arrows).

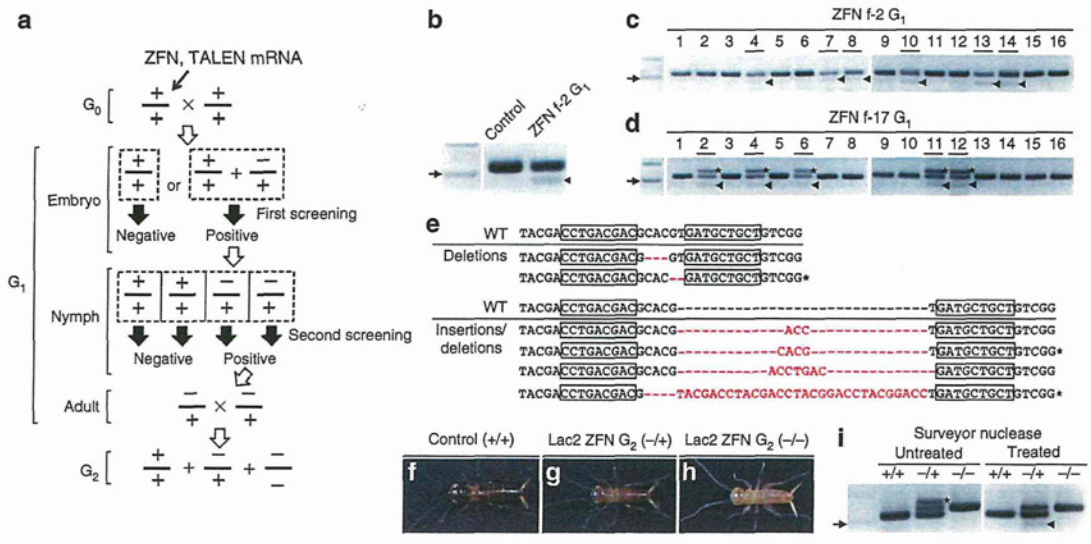

Figure 3 | Isolation of homozygous mutants after injection of *Gb'lac2* ZFN mRNAs into crickets. (**a**) An illustration of the scheme used to isolate homozygous mutations in an endogenous gene. Mutagenized G_0 adults were crossed to wild-type (WT) adults, and G_1 embryos were checked for heterozygous mutations in a first round of screening using the Surveyor nuclease. Positive G_1 individuals were developed into final-instar nymphs and subjected to a second round of screening with Surveyor nuclease assays. Positive G_1 adults were then crossed for each strain to obtain homozygous mutants in G_2 generation. (**b**) Germline mutations in G_0 crickets were detected in a first-round screening of G_1 embryos using Surveyor nuclease assays. The arrowhead indicates the product cleaved by the Surveyor nuclease in the f-2 line. Arrow indicates 200-bp size marker. (**c**,**d**) Isolation of heterozygous mutants from G_1 crickets in f-2 (**c**) and f-17 (**d**) lines detected in the second round of screening. Heterozygous mutant G_1 crickets were detected in a second round of screening of T3 legs from G_1 final-instar nymphs. Nymphs that harboured mutations caused by ZFNs are underlined. Arrowheads indicate the products generated from Surveyor nuclease assays. Asterisks indicate the presence of homoduplex PCR products from mutant alleles. Arrows indicate 200-bp size marker. (**e**) Sequence analysis of *Gb'lac2* mutant alleles induced by ZFNs. Wild-type sequences are shown above the mutant sequences containing deletions (indicated with dashes) and/or insertions (shown in red letters). Boxed sequences represent ZFN-binding sites. Asterisks indicate frame-shift mutations are present. (**f**–**h**) Phenotypes of G_2 heterozygous and homozygous mutant crickets 1 day after hatching. Control first-instar nymphs were coloured black until 1 day posthatching, while heterozygous mutants were still grey in colour and homozygous mutants were white. (**i**) Genotyping of G_2 heterozygous and homozygous mutants. In Surveyor nuclease assays, cleavage products were detected in heterozygous mutants (indicated with an arrowhead), but not in WT or homozygous mutants (right panel). The asterisk indicates heteroduplex PCR products from WT and mutant alleles were present. Arrow indicates 200-bp size marker.

Table 3 | Analysis of potential off-target sites of *Gb'lac2* ZFNs.

Off-target site sequence	Forward primer	Reverse primer	Product length (bp)
5′-CCTCACGACATCCTGGATCCTGCT-3′	5′-GCGTGGAGCTTATCGCAAGT-3′	5′-CGGGATGACACGTAGAACAGG-3′	121
5′-CCAGACGACTGAGATGTTGCTGCT-3′	5′-AACCGAAGCCCACTGTGTAAA-3′	5′-GCCCTCATGACTTGGCAGA-3′	168
5′-CGTGACGACGTAAAAGAAGCTGCT-3′	5′-CCGCCTCCTAACTCTGCGTA-3′	5′-TTAATGGCTCGGGTCCTTTG-3′	131
5′-CCTGATGACGATGCTGATGCTGAT-3′	5′-TGACCTTTTCCGTGAAAGATTTCCT-3′	5′-GACGGACACAAGTGGTCAGACATC-3′	145
5′-CCTGCCGACATTGCTGATGTTGCT-3′	5′-GTTTCCAAGACACTGAGCACTGAA-3′	5′-GGAAGGAATGGTTTACGCTAGACA-3′	160
5′-CCTGATGACAATGATGATGCTGAT-3′	5′-CCGAACCATCATTGCCTCTT-3′	5′-TGCATGCTTTGCCAGAGAAG-3′	138
5′-CATGACGACTTGCAAGAAGCTGCT-3′	5′-CGATGACGACGACAGAGACG-3′	5′-GCCTCCATACCCACACCTCA-3′	147
5′-CCTGACAACCCTGAGGACGCTGCT-3′	5′-TCAGCCCACGCTGAATTAAA-3′	5′-AACGAGCCCAAGCACTTGAC-3′	156
5′-CCTGACCACCTGACAGCTGCTGCT-3′	5′-CCCTTCCACCTCATCCACAT-3′	5′-CACATGCACGCCAATTACCT-3′	125

Mismatches to *Gb'lac2* ZFNs on-target site of each off-target sites are indicated by underlines. Grey colour shading indicates *Fok*I cleavage sites. The PCR using each set of primers was performed at an annealing temperature of 59 °C.

and without somatic mutations) were crossed with wild-type crickets. Genomic DNA was then extracted from a batch of embryos derived from each cross, and Surveyor nuclease-based assays were performed to detect germline-transmitted mutations (first-round screening; Fig. 3b). Founder crickets transmitting mutations were detected in ~47% of G_0 adults (Table 2). Embryos from the Surveyor-positive lines were then collected, hatched into nymphs, and reared. Genomic DNA was extracted from the T3 leg of 16 individual final-instar nymphs from each of the four positive lines identified in the first-round screening, and Surveyor nuclease-based assays were performed (second-round screening), followed by DNA sequencing (Fig. 3c,d). Surveyor-positive nymphs were obtained at a rate of 31–68% for each line, and these were reared to obtain G_1 adult crickets containing heterozygous mutant alleles. Sequencing of the ZFN-targeted locus in these mutants revealed that first round–positive lines often contained multiple mutant alleles (Fig. 3e).

To produce homozygous mutants, G_1 mutant siblings with identical mutations were mated. From these crosses, ~43% of hatched G_2 nymphs exhibited a lag in tanning (Fig. 3f,g), while 19% failed to tan (Fig. 3h). In the latter case, it appeared that a homozygous knockout of the *Gb'lac2* gene had been achieved. Homozygosity was confirmed with Surveyor nuclease-based genotyping (Fig. 3i) and sequencing. However, homozygous knockout crickets died in the first-instar stage.

To examine whether the ZFNs that were introduced caused off-target mutations, we performed a computational scan of a preliminary draft assembly of the *G. bimaculatus* genome (T.M. *et al.*, unpublished data). On the basis of nine sites identified as the most likely to represent off-target sites of ZFN cleavage (Table 3), assays of these nine loci in heterozygous (G_1) mutant genomes were performed independently for three mutant lines using Surveyor nuclease assays. No cleavage products were detected. Assuming that the efficiency of PCR amplification is equivalent between mutated and wild-type sequences at each of the loci, the Surveyor nuclease assay would be predicted to be able to detect mutations with an equivalent sensitivity as demonstrated with the *Gb'lac2* locus. If so, then our results indicate that unwanted mutations did not occur at the targeted genomic sites in these experiments. Furthermore, sequencing of potential off-target sites in the *Gb'lac2* mutant genomes supported the data obtained from Surveyor nuclease assays.

Gene knockout using TALENs. The gene knockout strategy developed for ZFNs proved to be robustly applicable to TALENs. To disrupt the *Gb'lac2* gene, a pair of TALENs targeted to the *Gb'lac2* locus was designed (Lac2-TALEN-L and Lac2-TALEN-R; Fig. 2a). These TALEN mRNAs were then injected into cricket eggs. In contrast with the toxicity associated with *Gb'lac2* ZFN mRNAs, the *Gb'lac2* TALEN mRNAs did not induce significant toxicity at 1 $\mu g\,\mu l^{-1}$ compared with embryos injected with Lac2-L alone (Fig. 4a). Thus, 1 $\mu g\,\mu l^{-1}$ was adopted as the concentration used for subsequent TALEN experiments. Of the fifth-instar G_0 larvae generated, ~17% represented somatic mutants with a mosaic cuticle pattern with and without tanning (Table 2). Furthermore, the results of Surveyor nuclease-based assays with G_1 embryos (first-round screening; Fig. 3a) suggested that mutations were induced in the targeted locus (Fig. 4b), and founder crickets represented ~17% of G_0 adults (Table 2). Following a screening of heterozygous mutants in G_1 nymphs (second-round screening; Figs. 3a and 4c,d) and mating of G_1 mutant siblings, homozygous *Gb'lac2* knockout crickets were obtained (Fig. 4e–g). Sequencing of the TALEN-targeted locus in these mutants revealed the presence of indels, which is consistent with the induction of error-prone NHEJ repair after introduction of a DSB (Fig. 4h).

Homozygous *Gb'lac2* knockout nymphs generated using TALENs died in the first-instar stage, similar to knockout nymphs generated using ZFNs. When TALEN-induced *Gb'lac2* mutants were crossed with ZFN-induced mutants, the resulting ZFN/TALEN homozygous *Gb'lac2* knockout nymphs exhibited the same lethal effect as ZFN/ZFN knockout nymphs. These results indicate that the lethality observed is specific for the *Gb'lac2* mutation, and is not due to mutations elsewhere in the genome. Moreover, we hypothesize that secondary consequences as a result of defects in the structural integrity of the cuticle in the absence of tanning are responsible for the lethality observed for homozygote crickets.

Discussion

Here an efficient approach for targeted mutagenesis and generation of biallelic (homozygous) knockouts in *G. bimaculatus* is reported. ZFNs and TALENs were used to induce germline mutations of exogenous and endogenous genes in the cricket genome. Via mutant screening steps using the Surveyor nuclease, we have successfully generated homozygous mutant crickets, which exhibit the knockout phenotype of the target gene, *Gb'lac2*. This is the first research in hemimetabolous insects to show effectiveness of ZFNs and TALENs, and their capacity to generate knockout animals. Thus, an important advance in the ability to directly manipulate the genome of a non-traditional animal model is described, and it only requires the microinjection of ZFN/TALEN mRNAs and the identification of mutants using a Surveyor nuclease assay. In this study, a marker gene with a clear epidermal defect phenotype was used. However, the approach presented in this paper is able to generate knockout animals independent of a specific genotype or phenotype. Accordingly, this method represents a practical, and generally accessible, technique by which to affect any locus in the cricket genome, or any other genome, given that delivery of mRNA can be successful.

The ZFN mRNA injection experiments performed resulted in 47–48% of fertile adults yielding mutant offspring. Combined with the sufficiently high frequency of NHEJ in crickets, it appears that

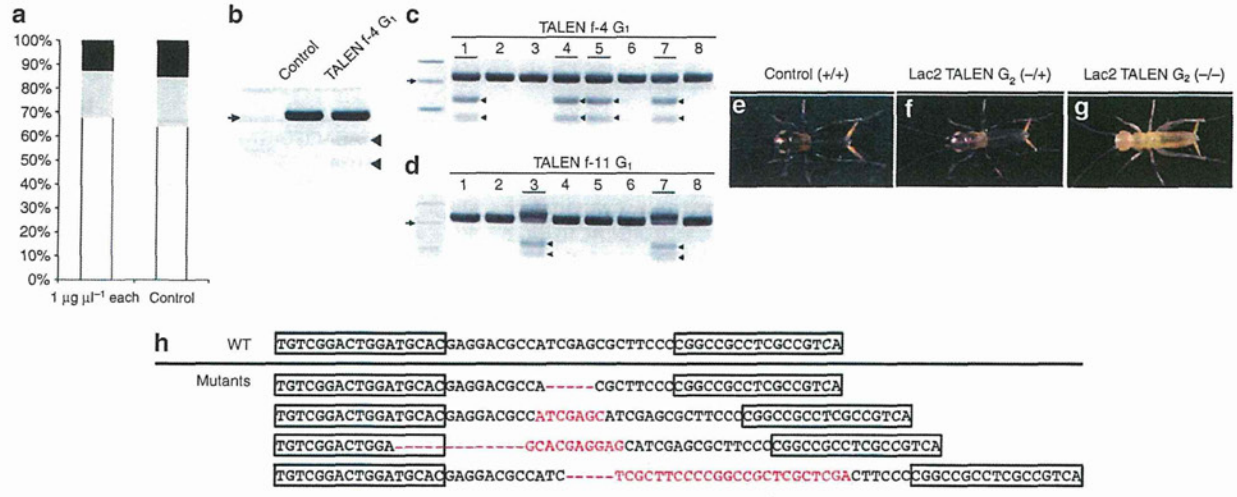

Figure 4 | Isolation of homozygous mutants induced by the microinjection of *Gb'lac2* TALEN mRNA into crickets. (**a**) Toxicity of *Gb'lac2* TALEN mRNAs in cricket embryos was detected. Percentages of dead (black), deformed (grey) and normal (white) embryos are shown at 2 days postinjection. The control included embryos injected with Lac2-L TALEN mRNA alone. The percentage of embryos that developed normally after microinjection of *Gb'lac2* TALEN mRNAs (68%, 82/121) was comparable to control (64%, 30/47). (**b**) Germline mutations in G_0 crickets were detected in a first-round screening of G_1 embryos. Arrowheads indicate the cleavage products generated in Surveyor nuclease assays of the f-4 line. Arrow indicates 200-bp size marker. (**c**,**d**) A second round of Surveyor nuclease assays was performed to identify heterozygous mutants present in G_1 crickets from the f-4 (**c**) and f-11 (**d**) lines. Adults that harboured mutations caused by TALENs are underlined, while arrowheads indicate cleavage products from Surveyor nuclease assays. Arrows indicate 200-bp size marker. (**e**–**g**) Phenotypes of G_2 heterozygous and homozygous *Gb'lac2* mutants generated with TALENs 1 day after hatching. Control first-instar nymphs were coloured black, while heterozygous mutants were still grey in colour and homozygous mutants were white. (**h**) Sequence analysis of *Gb'lac2* mutant alleles induced by TALENs. The wild-type (WT) sequence is shown above the mutant sequences containing deletions (indicated with dashes) and/or insertions (shown in red letters). Boxed sequences represent TALEN-binding sites.

our method can be used for: functional genomics in this species, disrupting specific coding sequences, and for targeting regulatory elements in the genome. In addition, the efficiency of generating founder animals using ZFNs is significantly higher than that observed for *Bombyx mori*[13], and is comparable to that of *Drosophila melanogaster* (Table 2)[11]. The disparity that exists between these species may be due to differences in the efficiency of mRNA incorporation into germline cells, and this may further depend on the mode of germ cell differentiation involved. In addition, differences in the binding affinity of ZFNs to target sequences may affect the efficiency of mutagenesis, especially as methods for ZFN design and screening differ between species.

Following the injection of ZFN mRNAs into embryos, dose-dependent toxicity was found to be significantly higher for *Gb'lac2*-targeted ZFNs than *eGFP*-targeted ZFNs. For example, lower concentrations of *Gb'lac2* ZFN mRNA yielded decreased rates of early embryonic lethality and malformation. These results are consistent with those previously reported for *Drosophila*[10,32], and suggest that dosage optimization for individual ZFN pairs is important for targeted mutagenesis, particularly to avoid unwanted genomic cleavage events. However, the target specificity demonstrated for *Gb'lac2*-targeted ZFNs injected at $1\,ng\,\mu l^{-1}$ indicates that specificity is sufficiently high, and no evidence of unwanted cleavage events were detected at nine other sites considered likely off-target genomic sites in *Gb'lac2* knockout crickets. While these data do not rule out the possibility that off-target ZFN cleavage events occurred at other loci, the specificity profile obtained is promising.

An advantage of using TALENs for genome editing is the greater flexibility in selecting target sequences versus ZFNs[33]. Our study is the first to demonstrate the capacity for TALENs to induce mutagenesis in insects other than *Drosophila*[24]. The rate of fertile adults that yielded mutant offspring in the present study (17%) also indicates that this method is suitable for practical use for cricket genome editing as well as ZFN-based mutagenesis. The frequency of NHEJ achieved in crickets used for TALEN experiments was lower than that of ZFN experiments performed for the same gene. However, mutation frequencies were not able to be directly compared between these experiments due to differences in the *Fok*I nuclease domains used (for example, heterodimer variants were used for ZFNs, and wild-type *Fok*I domains were used for TALENs). In addition, the targeted sequences were also different. In another report, engineered TALENs showed largely varying efficiencies of mutagenesis among 48 targeted sites in a single gene, or among 96 targeted genes in a human cell line[34]. Thus, it may be possible to achieve a higher efficiency of gene disruption using TALENs targeted to different sites.

Unlike RNAi-based technologies, ZFN/TALEN-based technologies are able to generate gene knockouts and gene knock-ins. In addition, the possibility of off-targeting effects can be more rigorously excluded by checking potential target sequences in the genome. However, preparation of custom double-stranded RNAs is generally easier than generating custom ZFNs/TALENs, and accessibility to phenotypes is another advantage of RNAi. For example, following the injection of double-stranded RNA into eggs, phenotypes can be observed within a few days, rather than waiting for the next generation. The systemic effect of RNAi also enables the observation of phenotypes at a specific developmental stage, or in a specific organ, as previously demonstrated in the cricket with nymphal or regeneration-dependent RNAi experiments[25–27]. Thus, if used in combination, both ZFN/TALEN-based genome editing and RNAi-based targeting have the potential to greatly promote functional genomics. For example, in the cricket where RNAi-based functional screening has rapidly identified candidate genes involved in many biological processes (for example, leg regeneration, early embryogenesis[25] and memory formation[35]), genome editing technologies can now be used to facilitate more detailed analyses of such genes using gene knock-out studies and the knock-in of reporter genes to obtain expression profiles.

While there are many beneficial and deleterious species of insects, the latter is associated with an enormous amount of

agricultural loss or fatal human disease. Currently, the well-established model insect systems that have been subject to sophisticated methods of genetic analysis and fully sequenced genomes (for example, fruitflies, red flour beetles and silkworms) are exclusively holometabolous (complete metamorphosis) species. However, many hemimetabolous species of insects (for example, aphids, cockroaches, crickets, grasshoppers) are significant agricultural pests or disease vectors. ZFNs/TALENs can be applied to the modification of genes responsible for deleterious traits in these insects, for example, to disrupt genes that facilitate the transmittal of pathogens, or to edit *cis*-regulatory regions of genes. Thus, the ability to edit the genomes of hemimetabolous insects using ZFNs/TALENs would facilitate the identification of new ways to address challenges posed by these insects, while avoiding the use of transgenic methods. This is in addition to contributing to genetic manipulation-based studies in other biological fields.

Methods

Animals. All adult and nymph two-spotted crickets, *G. bimaculatus*, were reared in plastic cases at 26–30 °C under a 10-h light, 14-h dark photoperiod. They were fed on artificial fish foods. For microinjections, fertilized eggs were collected on a wet kitchen towel and incubated at 28 °C in a plastic dish.

Design and screening of ZFNs. For designing ZFNs, the target sites of *eGFP* and *Gb'lac2* genes were scanned for positions where 6 bp lies between 5′-NNC-3′ and 5′-GNN-3′ triplets. The ZF proteins generated included three ZF domains, with each domain capable of recognizing 3 bp of DNA. Target site selection also included the requirement that sequences with single-nucleotide polymorphisms were excluded, as Surveyor nuclease assays would be able to detect single-nucleotide polymorphisms as well as ZFN- or TALEN-induced mutations.

Gb'lac2 ZFNs were designed to cleave a region encoding the catalytic domain of the *Gb'lac2* gene. To screen for functional ZFNs, a bacterial one-hybrid system was used in combination with an SSA assay as described previously[17]. Briefly, randomized libraries of ZFs, containing fusion proteins of three-finger ZF arrays and the omega subunit of RNA polymerase, were co-transfected with HIS3 reporter vectors, containing the target sequences for ZF arrays, into the bacterial strain, US0D hisBDpyrFDrpoZ. Transfected bacteria were then plated on histidine-deficient plates with the HIS3 inhibitor, 3-amino-1,2,4-triazole. In SSA assays, a ZFN construct and a reporter construct containing a luciferase gene split into two inactive fragments by insertion of a stop codon and a pair of target sites were co-transfected into cultured cells. When a DSB at the target site is induced by a ZFN homodimer, SSA occurs between the homologous regions of the inactive fragments, thereby producing an active luciferase gene. *eGFP* ZFNs were assembled using DD/RR *Fok*I heterodimer variants, while *Gb'lac2* ZFNs were assembled using DS/RR heterodimer *sharky* variants[29,31].

The design, construction and validation of TALENs targeting the *Gb'lac2* gene (*Gb'lac2* TALENs L and R) were performed by Cellectis Bioresearch (Paris, France). Each TALEN recognized a 17-bp target site, and these sites were 23 bp apart.

mRNA synthesis and microinjections into *Gryllus* eggs. *In vitro* transcription of capped mRNA was performed using an mMESSAGE mMACHINE kit (Ambion, Austin, TX, USA) according to the manufacturer's instructions. Following ethanol precipitation, mRNAs were suspended in an appropriate volume of water to achieve a final concentration of 1 $\mu g\,\mu l^{-1}$ for *eGFP* ZFNs and *Gb'lac2* TALENs and 1 $ng\,\mu l^{-1}$ for *Gb'lac2* ZFNs. To perform microinjections of mRNA, cricket eggs were collected within 1 h of being laid and were used within 4 h of collection. The eggs were lined up on double-sided adhesive tape attached to a microscope slide after treatment with 70% ethanol for 10 s and wash. Solution containing mRNA was backloaded into a glass needle and injected into each egg at 20% in the egg length[26].

Analysis of mutations using Surveyor nucleases. Primer pairs amplified a region of 400 and 210 bp containing the *eGFP* and *Gb'lac2* target sites, respectively. To detect *eGFP*- or *Gb'lac2*-ZFN-induced mutations in G_0 embryos, we extracted genomic DNA of 25 embryos at 7 or 2 days after injection, respectively, and used them for the Surveyor nuclease assays. For the first round of screening in the ZFN/TALEN experiments, genomic DNA of 25 G_1 embryos at 7 days after egg laying were used in each line. For the second round of Surveyor nuclease assays, genomic DNA was extracted from T3 legs of G_1 final-instar nymphs. To allow complementary but mismatched strands to anneal, PCR products (10 µl) were incubated at 95 °C for 5 min, 95 °C for 85 °C at $-2\,°C\,s^{-1}$ and 85 °C to 25 °C at $-0.1\,°C\,s^{-1}$. Nuclease S (0.5 µl) and Enhancer S (0.5 µl) (Surveyor Mutation Detection Kit, Transgenomic, Omaha, NE, USA) were then added and samples were incubated at 42 °C for 20 min to digest the annealed PCR products at the sites of mismatch. Nuclease S-digested PCR products were analysed by agarose gel electrophoresis.

References

1. Rothstein, R. J. One-step gene disruption in yeast. *Methods Enzymol.* **101,** 202–211 (1983).
2. Rong, Y. S. & Golic, K. G. in *Insect Transgenesis Methods and Applications* (eds Handler, A. M., James, A. A.) 53–75 CRC Press, 2000.
3. Capecchi, M. R. Gene targeting in mice: functional analysis of the mammalian genome for the twenty-first century. *Nat. Rev. Genet.* **6,** 507–512 (2005).
4. Porteus, M. H. & Carroll, D. Gene targeting using zinc finger nucleases. *Nat. Biotechnol.* **23,** 967–973 (2005).
5. Miller, J. C. *et al.* A TALE nuclease architecture for efficient genome editing. *Nat. Biotechnol.* **29,** 143–148 (2011).
6. Kim, Y. G., Cha, J. & Chandrasegaran, S. Hybrid restriction enzymes: zinc finger fusions to *Fok*I cleavage domain. *Proc. Natl Acad. Sci. USA* **93,** 1156–1160 (1996).
7. Carroll, D., Morton, J. J., Beumer, K. J. & Segal, D. J. Design, construction and *in vitro* testing of zinc finger nucleases. *Nat. Protoc.* **1,** 1329–1341 (2006).
8. Moscou, M. J. & Bogdanove, A. J. A simple cipher governs DNA recognition by TAL effectors. *Science* **326,** 1501 (2009).
9. Smith, J. *et al.* Requirements for double-strand cleavage by chimeric restriction enzymes with zinc finger DNA-recognition domains. *Nucleic Acids Res.* **28,** 3361–3369 (2000).
10. Bibikova, M., Golic, M., Golic, K. G. & Carroll, D. Targeted chromosomal cleavage and mutagenesis in *Drosophila* using zinc-finger nucleases. *Genetics* **161,** 1169–1175 (2002).
11. Beumer, K. J. *et al.* Efficient gene targeting in *Drosophila* by direct embryo injection with zinc-finger nucleases. *Proc. Natl Acad. Sci. USA* **105,** 19821–19826 (2008).
12. Bozas, A., Beumer, K. J., Trautman, J. K. & Carroll, D. Genetic analysis of zinc-finger nuclease-induced gene targeting in *Drosophila*. *Genetics* **182,** 641–651 (2009).
13. Takasu, Y. *et al.* Targeted mutagenesis in the silkworm *Bombyx mori* using zinc finger nuclease mRNA injection. *Insect Biochem. Mol. Biol.* **40,** 759–765 (2010).
14. Doyon, Y. *et al.* Heritable targeted gene disruption in zebrafish using designed zinc-finger nucleases. *Nat. Biotechnol.* **26,** 702–708 (2008).
15. Mashimo, T. *et al.* Generation of knockout rats with X-linked severe combined immunodeficiency (X-SCID) using zinc-finger nucleases. *PLoS ONE* **5,** e8870 (2010).
16. Rémy, S. *et al.* Zinc-finger nucleases: a powerful tool for genetic engineering of animals. *Transgenic Res.* **19,** 363–371 (2010).
17. Ochiai, H. *et al.* Targeted mutagenesis in the sea urchin embryo using zinc-finger nucleases. *Genes Cells* **15,** 875–885 (2010).
18. Wood, A. J. *et al.* Targeted genome editing across species using ZFNs and TALENs. *Science* **333,** 307 (2011).
19. Young, J. J. *et al.* Efficient targeted gene disruption in the soma and germ line of the frog *Xenopus tropicalis* using engineered zinc-finger nucleases. *Proc. Natl Acad. Sci. USA* **108,** 7052–7057 (2011).
20. Carbery, I. D. *et al.* Targeted genome modification in mice using zinc-finger nucleases. *Genetics* **186,** 451–459 (2010).
21. Meyer, M., de Angelis, M. H., Wurst, W. & Kühn, R. Gene targeting by homologous recombination in mouse zygotes mediated by zinc-finger nucleases. *Proc. Natl Acad. Sci. USA* **107,** 15022–15026 (2010).
22. Tesson, L. *et al.* Knockout rats generated by embryo microinjection of TALENs. *Nat. Biotechnol.* **29,** 695–696 (2011).
23. Sander, J. D. *et al.* Targeted gene disruption in somatic zebrafish cells using engineered TALENs. *Nat. Biotechnol.* **29,** 697–698 (2011).
24. Liu, J. *et al.* Efficient and specific modifications of the *Drosophila* genome by means of an easy TALEN strategy. *J. Genet. Genomics* **39,** 209–215 (2012).
25. Mito, T., Nakamura, T., Bando, T., Ohuchi, H. & Noji, S. The advent of RNA interference in entomology. *Entomol. Sci.* **14,** 1–8 (2010).
26. Nakamura, T. *et al.* Imaging of transgenic cricket embryos reveals cell movements consistent with a syncytial patterning mechanism. *Curr. Biol.* **20,** 1641–1647 (2010).
27. Hamada, A. *et al.* Loss-of-function analyses of the fragile X-related and dopamine receptor genes by RNA interference in the cricket *Gryllus bimaculatus*. *Dev. Dyn.* **238,** 2025–2033 (2009).
28. Meng, X., Noyes, M. B., Zhu, L., Lawson, N. D. & Wolfe, S. A. Targeted gene inactivation in zebrafish using engineered zinc finger nucleases. *Nat. Biotechnol.* **26,** 695–701 (2008).
29. Szczepek, M. *et al.* Structure-based redesign of the dimerization interface reduces the toxicity of zinc-finger nucleases. *Nat. Biotechnol.* **25,** 786–793 (2007).
30. Miller, J. C. *et al.* An improved zinc-finger nuclease architecture for highly specific genome editing. *Nat. Biotechnol.* **25,** 778–785 (2007).
31. Guo, J., Gaj, T. & Barbas, C. F. 3rd. Directed evolution of an enhanced and highly efficient FokI cleavage domain for zinc finger nucleases. *J. Mol. Biol.* **400,** 96–107 (2010).
32. Beumer, K., Bhattacharyya, G., Bibikova, M., Trautman, J. K. & Carroll, D. Efficient gene targeting in *Drosophila* with zinc-finger nucleases. *Genetics* **172,** 2391–2403 (2006).
33. Cermak, T. *et al.* Efficient design and assembly of custom TALEN and other TAL effector-based constructs for DNA targeting. *Nucleic Acids Res.* **39,** e82 (2011).

34. Reyon, D. *et al.* FLASH assembly of TALENs for high-throughput genome editing. *Nat. Biotechnol.* **30,** 460–465 (2012).
35. Takahashi, T. *et al.* Systemic RNA interference for the study of learning and memory in an insect. *J. Neurosci. Methods* **179,** 9–15 (2009).

Acknowledgements
This work was supported by JSPS KAKENHI (23687033) to T.M., (23710217) to T.B., (22770057/23111521) to T.N., (22124003/22370080) to T.M., H.Ohu. and S.N., and (20200006) to T.Y.

Author contributions
S.N., T.M., T.W. and T.Y. designed research. T.W., H.Och., T.S., N.H. and H.H. performed experiments. T.W., T.N., T.B., H.Ohu., S.N., T.Y. and T.M. analysed data. T.M. and T.W. wrote the paper and all co-authors contributed in the form of discussion and critical comments.

Addditional informations
Competing financial interests: The authors declare no competing financial interests.

Reprints and permission information is available online at http://npg.nature.com/reprintsandpermissions/

How to cite this article: Watanabe, T. *et al.* Non-transgenic genome modifications in a hemimetabolous insect using zinc-finger and TAL effector nucleases. *Nat. Commun.* 3:1017 doi: 10.1038/ncomms2020 (2012).

THE JOURNAL OF BIOLOGICAL CHEMISTRY VOL. 287, NO. 46, pp. 38716–38728, November 9, 2012

Matrix Metalloproteinase-13 (MMP-13) Directly and Indirectly Promotes Tumor Angiogenesis*

Received for publication, April 17, 2012, and in revised form, September 10, 2012 Published, JBC Papers in Press, September 19, 2012, DOI 10.1074/jbc.M112.373159

Yasusei Kudo[‡§1], Shinji Iizuka[‡], Maki Yoshida[‡], Takaaki Tsunematsu[‡], Tomoyuki Kondo[§], Ajiravudh Subarnbhesaj[‡], Elsayed M. Deraz[‡], Samadarani B. S. M. Siriwardena[‡], Hidetoshi Tahara[¶], Naozumi Ishimaru[§], Ikuko Ogawa[‖], and Takashi Takata[‡2]

From the [‡]Department of Oral and Maxillofacial Pathobiology and [¶]Department of Cellular and Molecular Biology, Graduate School of Biomedical Sciences, Hiroshima University, and the [‖]Center of Oral Clinical Examination, Hiroshima University Hospital, Hiroshima 734-8553, Japan and the [§]Department of Oral Molecular Pathology, Institute of Health Biosciences, The University of Tokushima Graduate School, Tokushima 770-8504, Japan

Background: Angiogenesis is an important step in the metastatic cascade of tumors.
Results: MMP-13 itself as well as VEGF-A secretion from fibroblasts promotes angiogenesis. Indeed, MMP-13 is well correlated with blood vessel density in human cancer tissues.
Conclusion: MMP-13 can be a marker for prediction of malignant behaviors and a therapeutic target in cancer.
Significance: This work provides new insights regarding the role of MMP-13 in tumor angiogenesis.

Matrix metalloproteinases (MMPs) are extracellular zinc-dependent endopeptidases involved in the degradation and remodeling of extracellular matrix in physiological and pathological processes. MMPs also have a role in cell proliferation, migration, differentiation, angiogenesis, and apoptosis. We previously identified cancer invasion-related factors by comparing the gene expression profiles between parent and the highly invasive clone of cancer cells. Matrix metalloproteinase-13 (MMP-13) was identified as a common up-regulated gene by cancer invasion-related factors. Although MMP-13 slightly promoted tumor invasion, we found that MMP-13 was involved in tumor angiogenesis. Conditioned medium from MMP-13-overexpressing cells promoted capillary formation of immortalized human umbilical vein endothelial cells. Furthermore, treatment with recombinant MMP-13 protein enhanced capillary tube formation both *in vitro* and *in vivo*. MMP-13-promoted capillary tube formation was mediated by activation of focal adhesion kinase and ERK. Interestingly, MMP-13 promoted the secretion of VEGF-A from fibroblasts and endothelial cells. By immunohistochemical analysis, we found a possible correlation between MMP-13 expression and the number of blood vessels in human cancer cases. In summary, these findings suggest that MMP-13 may directly and indirectly promote tumor angiogenesis.

The process of metastasis consists of sequential and selective steps, including proliferation, induction of angiogenesis, detachment, motility, invasion into circulation, aggregation and survival in the circulation, cell arrest in distant capillary beds and extravasation into organ parenchyma (1, 2). Induction of angiogenesis is considered one of the important steps in the metastatic cascade of tumors. It is widely accepted that tumor growth and metastasis are angiogenesis-dependent, and hence, blocking angiogenesis could be a strategy to arrest tumor growth (3). The "angiogenic switch" is "off" when the effect of proangiogenic molecules is balanced by that of anti-angiogenic molecules, and is "on" when the net balance is tipped in favor of angiogenesis (4, 5). Pro- and anti-angiogenic molecules can be emanated from cancer cells, endothelial cells, stromal cells, blood, and the extracellular matrix (ECM)[3] (6). Their relative contribution is likely to change with tumor type and site. It is also likely to change with tumor growth, regression and relapse. However, the interplay between environmental and genetic mechanisms influencing tumor angiogenesis and growth is a complex and largely unresolved matter.

The ECM undergoes significant remodeling during tumor progression and this is mediated largely by the extracellular proteinases, particularly the matrix metalloproteinases (MMPs), and the major source of these is from the stromal cells (7). MMPs represent a family of zinc-dependent proteinases, which are able to degrade ECM components such as collagens and proteoglycans and have a role in normal development and tissue damage in various pathophysiological conditions involving arthritis, wound healing, and tumor development (8). MMPs can be classified into subgroups, including collagenases, stromelysins, gelatinases, and membrane-type MMPs (9). MMPs have been implicated in the promotion of tumor inva-

* This work was supported by grants-in-aid from the Ministry of Education, Science, and Culture of Japan (to Y. K. and T. Ta.), a research fellowship for Young Scientists and the Excellent Young Researchers Overseas Visit Program from the Japan Society for the Promotion of Science (to S. I. and T. Ts.), and a Kurozumi Memorial Foundation grant (to Y. K.).

[1] To whom correspondence may be addressed: Dept. of Oral Molecular Pathology, Institute of Health Biosciences, The University of Tokushima Graduate School, Tokushima, 3-18-15 Kuramoto, Tokushima 770-8504, Japan. Fax: 81-88-633-7328; E-mail: yasusei@tokushima-u.ac.jp.

[2] To whom correspondence may be addressed: Dept. of Oral and Maxillofacial Pathobiology, Division of Frontier Medical Science, Graduate School of Biomedical Sciences, Hiroshima University, 1-2-3 Kasumi, Minami-ku, Hiroshima 734-8553, Japan. Fax: 81-82-257-5619; E-mail: ttakata@hiroshima-u.ac.jp.

[3] The abbreviations used are: ECM, extracellular matrix; MMP, matrix metalloproteinase; VEGF, vascular endothelial growth factor; FAK, focal adhesion kinase; HUVEC, human umbilical vein endothelial cell; HNSCC, head and neck squamous cell carcinoma; TGF-β, transforming growth factor-β: α-SMA, α-smooth muscle actin.

sion and metastasis for decades (10). It is now evident that MMP function is more complex than initially thought, given that these enzymes do more than degrade physical barriers. MMPs also affect multiple signaling pathways that modulate the biology of the cell in normal physiological processes and in disease. It is now evident that some MMPs such as MMP-1, -2, -3, -7, -9, -14, and -16 can contribute to distinct vascular events in tumors (11). Among them, MMP-9, conveyed by inflammatory cells, has a distinct role in tumor angiogenesis, mainly regulating the bioavailability of VEGF. MMP-9 enables an angiogenic switch by making sequestered VEGF bioavailable for its receptor VEGFR-2 in pancreatic islet tumors (12). In addition, the direct cleavage of matrix-bound VEGF by MMP-3, -7, -9, or -16 results in modified VEGF molecules with altered bioavailability, which changes the vascular patterning of tumors *in vivo* (13). However, the degradation of ECM components and other extracellular molecules may generate fragments with new bioactivities that inhibit angiogenesis (14). Thus, MMPs have dual functions as inhibiting and promoting angiogenesis, and the effects of MMPs on angiogenesis might be diverse.

It has recently been shown that a repair of bone fracture in MMP-13-deficient mice is delayed, which suggests a critical role of MMP-13 in the process of angiogenesis during the healing of fracture (15). Additionally, chicken MMP-13 was shown to directly contribute to neovascularization, which clearly extends the physiologic role of MMP-13 associated with cartilage and bone resorption to collagen remodeling in the angiogenic process (16). MMP-13 is known as collagenase-3 and is active against a wide variety of ECM components (17). Moreover, high expression of MMP-13 has been related to tumor behavior and prognosis (18). Recently, it has been shown that MMP-13 produced from stromal fibroblasts promotes angiogenesis through increased protein level of VEGF and VEGFR-2 in cancer invasive area (19). Here, we found that MMP-13 produced by cancer cells directly and indirectly promoted tumor angiogenesis.

EXPERIMENTAL PROCEDURES

Reagents—Active form of recombinant human MMP-13, which truncated from the C terminus was obtained from Chondrex, Inc. (Redmond, WA). This recombinant protein was made using the pET vector system in *Escherichia coli*. Recombinant TGF-β and ERK inhibitor, U0126 was obtained from R&D Systems (Minneapolis, MN). Focal adhesion kinase (FAK) inhibitor, FAK inhibitor 14, was obtained from Santa Cruz Biotechnology (Santa Cruz, CA). MMP-13 inhibitor, CL82198, was obtained from Merck Millipore (Darmstadt, Germany).

Cell Lines and Culture Conditions—Head and neck squamous cell carcinoma (HNSCC) cell lines (HCS2, HSC3, HSC4, Ca-9-22, Ho-1-N-1, and Ho-1-U-1) were provided by the Japanese Collection of Research Bioresources Cell Bank. These cells were maintained in RPMI 1640 (Nacalai tesque, Inc., Kyoto, Japan) supplemented with 10% heat-inactivated FBS (Invitrogen) and 100 units/ml penicillin-streptomycin (Invitrogen) under the condition of 5% CO_2 in air at 37 °C. Immortalized human umbilical vein endothelial cells (HUVECs; HuhT1 cells) were used in this study. HuhT1 cells were previously established by transfection with human telomerase reverse transcriptase (20). HuhT1 cells was maintained in HuMedia-EG2 (Kurabo, Okayama, Japan) under the condition of 5% CO_2 in air at 37 °C. Normal fibroblasts were obtained from gingival tissues using standard explant techniques (21). The tissues were obtained undergoing routine dental surgery in the Department of Oral Surgery (Hiroshima University Hospital). Normal fibroblasts were maintained in DMEM supplemented with 10% FBS. Only cells between passages three and five were used in this study.

RT-PCR—Using RNeasy mini kit (Qiagen, Hilden, Germany), total RNA from cultures of confluent cells was isolated. These isolates were quantified and their purity was evaluated by spectrophotometer. The cDNA was synthesized from 1 μg of total RNA according to ReverTra Dash (Toyobo Biochemicals, Tokyo, Japan). We used the following primers: human MMP-13, 5′-ttgagctggactcattgtcg-3′ (forward) and 5′-ggagcctctcagtcatggag-3′ (reverse); human glyceraldehyde-3-phosphate dehydrogenase (GAPDH), 5′-tccaccaccctgttgctgta-3′ (forward) and 5′-accacagtccatgccatcac-3′ (reverse). Aliquots of total cDNA were amplified with 1.25 units of rTaq-DNA polymerase (Qiagen), and this amplification was done in a thermal cycler (MyCyler, Bio-Rad, Richmond, CA) for 30 cycles after initial 30 s of denaturation at 94 °C, annealing for 30 s at 60 °C, and extension for 1 min at 72 °C in all primers used. The amplification reaction products were resolved on 1.2% agarose/TAE gels (Nacalai tesque), electrophoresed at 100 mV, and then finally visualized by using ethidium bromide.

Generation of MMP-13-overexpressing Cells—pcDNA3.1-FLAG-MMP-13 expression vector was kindly provided by Dr. Michael Byrne (Harvard Medical School). We transfected MMP-13 into HSC3 cells. Then, G418 (300 μg/ml; Invivogen, San Diego, CA) was added to the culture medium after 48 h of transfection. After 2 weeks of G418 selection, we obtained the stable pool clones. Cell transfections were performed using FuGENE 6HD (Roche Applied Science) according to the manufacturer's instruction. Conditioned media were collected after incubation with RPMI without FBS for 2 days.

Silencing by siRNA—Logarithmically growing HSC4 and Ho-1-N-1 cells were seeded at a density of 10^5 cells/dish (6 cm) and transfected with 20 nM siRNA by using Oligofectamine® RNAi MAX (Invitrogen), according to the manufacturer's instructions. Forty-eight hours after transfection, the cells were prepared and analyzed by Western blot analysis. At the same time, we changed to new medium, incubated for 48 h, and collected the conditioned medium. The following siRNA oligonucleotides were obtained from B-Bridge International, Inc. (Mountain View, CA): MMP-13, gaugaaaccuggacaaguaTT. A scrambled sequence without significant homology to rat, mouse, or human gene sequences was used as a control.

Western Blot Analysis—Western blotting was carried out as described previously (22). The protein concentrations were measured by Bradford protein assay (Bio-Rad). Twenty μg of protein was subjected to 10% polyacrylamide gel electrophoresis, followed by electroblotting onto a nitrocellulose filter. For detection of the immunocomplex, the ECL Western blotting detection system (Amersham Biosciences) was used. Anti-MMP-13 monoclonal antibody (Fuji Company Industries, Tokyo, Japan), anti-FLAG monoclonal antibody (Sigma), and

anti-β-actin monoclonal antibody (Sigma), α-smooth muscle actin (α-SMA), anti-phospho-FAK (Tyr-576/Tyr-577) monoclonal antibody (Cell Signaling Technology, Beverly, MA), anti-phospho-Src (Tyr-416) polyclonal antibody (Cell Signaling Technology), anti-phospho-ERK (Thr-202/Tyr-204) monoclonal antibody (Santa Cruz Biotechnology, Santa Cruz, CA), anti-FAK polyclonal antibody (Cell Signaling Technology), anti-Src polyclonal antibody (Cell Signaling Technology), and anti-ERK monoclonal antibody (Cell Signaling Technology) were used. For detection of phosphorylated proteins, membranes were blocked with 3% milk/TBS-T and incubated with phospho-specific antibodies overnight at 4 °C. After washing in TBS-T, membranes were incubated with specific secondary antibodies, and the proteins were visualized as described previously.

MMP-13 Activity—The MMP-13 activity was determined by a MMP-13 inhibitor assay kit (Chondrex, Inc., Redmond, WA, distributed by IWAI Chemicals Company, Japan, catalog no. 3003). A designate reaction was performed in the 96-well

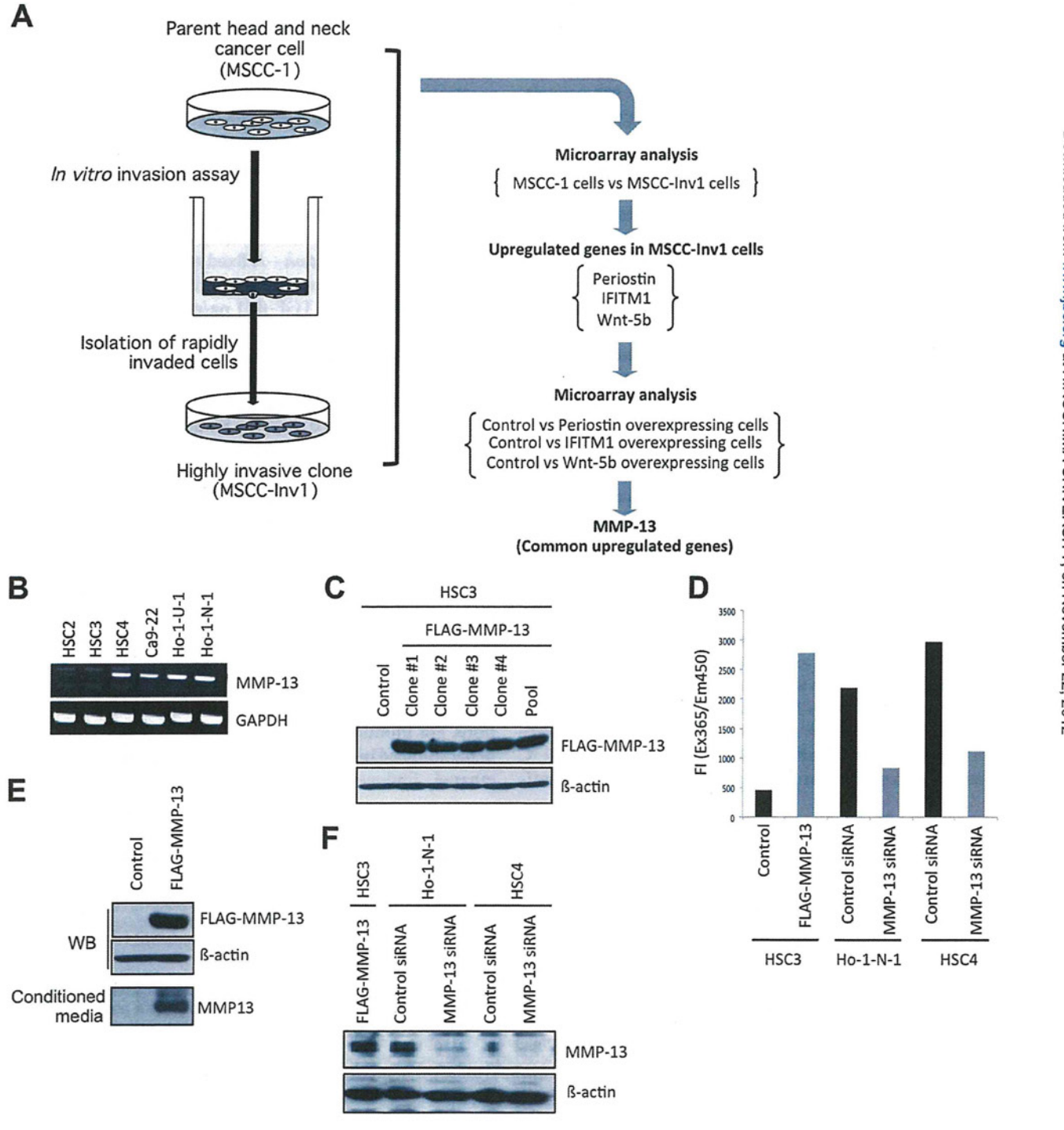

microtiter plate according to the manufacturer's instructions. The assay procedure was separated into two stages. First, diluted recombinant human MMP-13 (10 μg/ml) with dilution buffer B or conditioned medium (from control cells, MMP-13-overexpressing cells or MMP-13 siRNA-treated cells) was activated by adding 5 μl of aminophenylmercuric acetate at 35 °C for 60 min. Second, appropriate amounts of test samples with or without several inhibitors (U0126, FAK inhibitor 14 and CL82198) that diluted by solution B and reaction buffer to the wells were added to adjust the final volume to 160 μl. The reaction was initiated by adding 100 μl of substrate solution to each well. The collagenase reaction was stopped by adding 10 μl of the stop solution to each well after incubating at room temperature for ~30 min. The reaction fluorescence intensity was determined at $\lambda_{emission}$ = 450 nm and $\lambda_{excitation}$ = 345 nm with Varioskan Flash (Thermo Scientific). The MMP-13 activity was determined by comparing with a standard response curve using buffer instead of inhibitor in similar conditions. All assays were carried out in three replications.

Migration Assay—Migration activity was measured by the use of a 24-well cell culture insert with 8-μm pores (Falcon Becton Dickinson). The lower compartment contained 0.5 ml of conditioned medium or serum-free medium with or without 100 ng/ml of recombinant MMP-13. After trypsinization, 5×10^4 cells were resuspended in 100 μl of serum-free medium and placed in the upper compartment of the cell culture insert for 4 h. To examine the activity of migration, the cells that had penetrated onto the lower side of the filter were fixed with formalin and stained with hematoxylin. These were assayed three times.

In Vitro Angiogenesis by HUVECs—An angiogenesis assay kit obtained from Kurabo (Osaka, Japan) was used according to the manufacturer's instructions with minor modifications (23). HUVECs were treated with conditioned medium from MMP-13-overexpressing cells or control cells (1:1 mixture with the medium). HUVECs were also treated with different concentrations of recombinant MMP-13 protein (0, 50, 100 and 200 ng/ml). VEGF-A (2 μg/ml) was used as a positive control, and suramin (1 mM) was used as a negative control. We examined three wells/data point in a single experiment. The media were changed every 3 days. After 12 days, the cells were fixed at room temperature with cold 70% ethanol for 30 min. The cells were incubated with the anti-human CD31 antibody for 1 h at 37 °C and further with an alkaline phosphatase-conjugated goat anti-mouse IgG antibody. Visualization was achieved with 5-bromo-4-chloro-3-indolyl phosphate-nitrobluetetrazolium. Capillary tube score was estimated with the Chalkley count method under a bright-field microscope (24).

Rat Aortic Ring Angiogenesis Assay—The effect of samples on angiogenesis was studied by culturing aortic explants in three-dimensional matrix gels according to the protocol described by Bauer *et al.* (25). Thoracic aorta was excised from 7-week-old male Sprague-Dawley rat, and the fibroadipose tissue was removed. The aorta was sectioned into 1-mm-long cross-sections, rinsed with EBM-2 medium (Lonza, Walkersville, MD), placed on the Matrigel-coated wells, covered with additional 50 μl of Matrigel, and allowed to form a gel for more than 30 min at 37 °C, 5% CO_2. Afterward, control was treated with EBM-2 medium only, and the test sample was treated with EBM-2 medium containing recombinant MMP-13 protein. Each medium was added every other day. All assays were performed by using five aortic rings per sample. Aortic rings were photographed on day 15. The area of angiogenic sprouting was calculated using Image-Pro Plus software program (Media Cybernetics). Microvessel densities were reported in square pixels.

VEGF-A Quantification—A fixed number of fibroblasts cultured in medium without FBS were treated with MMP-13 (0, 10 and 50 ng/ml) and/or TGF-β (1 ng/ml) for 24 h. The concentration of VEGF-A in the culture medium was quantified with commercial ELISA kit according to the manufacturers' instructions (Pierce Biotechnology, Rockford, IL).

Tissue Samples—Sixty-seven tissue samples of human HNSCC were retrieved from the Surgical Pathology Registry of University of Peradeniya and Oral and Maxillofacial unit, Kandy Hospital, after being approved by the Ethical Committee of each institution. Informed consent obtained from all patients was verbal for this study, and then signature was obtained from all patients. Sixty-seven Sri Lankan HNSCC cases (42 male, nine female and 16 unknown; average age was 50.2 ± 13.2) were surgically resected from 1998 to 2004 before radiochemotherapy. Clinical information including metastasis was gathered from surgical records of the patients. Tissues were fixed in 10% buffered formalin and embedded in paraffin.

Immunohistochemistry—Tumor tissues were fixed in 10% formalin, embedded in paraffin, and cut into 4-μm thick sections. For immunohistochemical staining, tissue sections were deparaffinized in xylene and rehydrated in descending grades of ethanol. Endogenous peroxidase activity was blocked with

FIGURE 1. **Identification of MMP-13.** *A*, schema shows the strategy to identify MMP-13. Periostin, IFITM1, and Wnt-5b are identified as the invasion-related molecules by comparing the gene expression profile between the parent (MSCC-1 cells) and a highly invasive clone (MSCC-Inv1 cells). To identify common up-regulated genes, we compared the gene expression profiles of control *versus* periostin-overexpressing cells, control *versus* IFITM1-overexpressing cells, and control *versus* Wnt-5b-overexpressing cells. MMP-13 is commonly up-regulated among periostin-, IFITM1-, and Wnt-5b-overexpressing cells. *B*, expression of MMP-13 in HNSCC cell lines. Expression of MMP-13 mRNA in six HNSCC cell lines: HSC2, HSC3, HSC4, Ca-9-22, Ho-1-N-1, and Ho-1-U-1 was examined by RT-PCR. GAPDH was used as a loading control. *C*, generation of MMP-13-overexpressing cells. pcDNA3.1-FLAG-MMP13 was transfected into HSC3 cells. After selection, we obtained four stable clones and one stable pool clone of MMP-13-overexpressing cells. Ectopic expression of MMP-13 was examined by immunoblotting with an anti-FLAG antibody. In further experiments, clone 1 was used. *D*, MMP-13 ability was determined by a MMP-13 inhibitor assay kit as described under "Experimental Procedures." Conditioned medium was collected from control HSC3, MMP-13-overexpressing HSC3, control Ho-1-N-1, MMP-13 siRNA-treated Ho-1-N-1, control HSC4, and MMP-13 siRNA-treated HSC4 cells. The reaction was initiated by adding 100 μl of substrate solution, and the reaction fluorescence intensity was determined at $\lambda_{emission}$ = 450 nm and $\lambda_{excitation}$ = 345 nm. The graph shows fluorescence intensity. All assays were carried out in three replications. *E*, ectopic expression of FLAG-MMP-13 was examined by immunoblotting with an anti-FLAG antibody. β-Actin expression was used as a loading control. Expression of MMP-13 in condensed conditioned medium was detected by immunoblotting with an anti-MMP-13 antibody. *F*, MMP-13 knockdown in HSC4 and Ho-1-N-1 cells. MMP-13 siRNA was transfected into HSC4 and Ho-1-N-1 cells. A scrambled sequence that does not show significant homology to rat, mouse, or human gene sequences was used as a control. After 48 h, cells were collected, and MMP-13 expression was examined by Western blot (*WB*) analysis. β-Actin expression was used as a loading control.

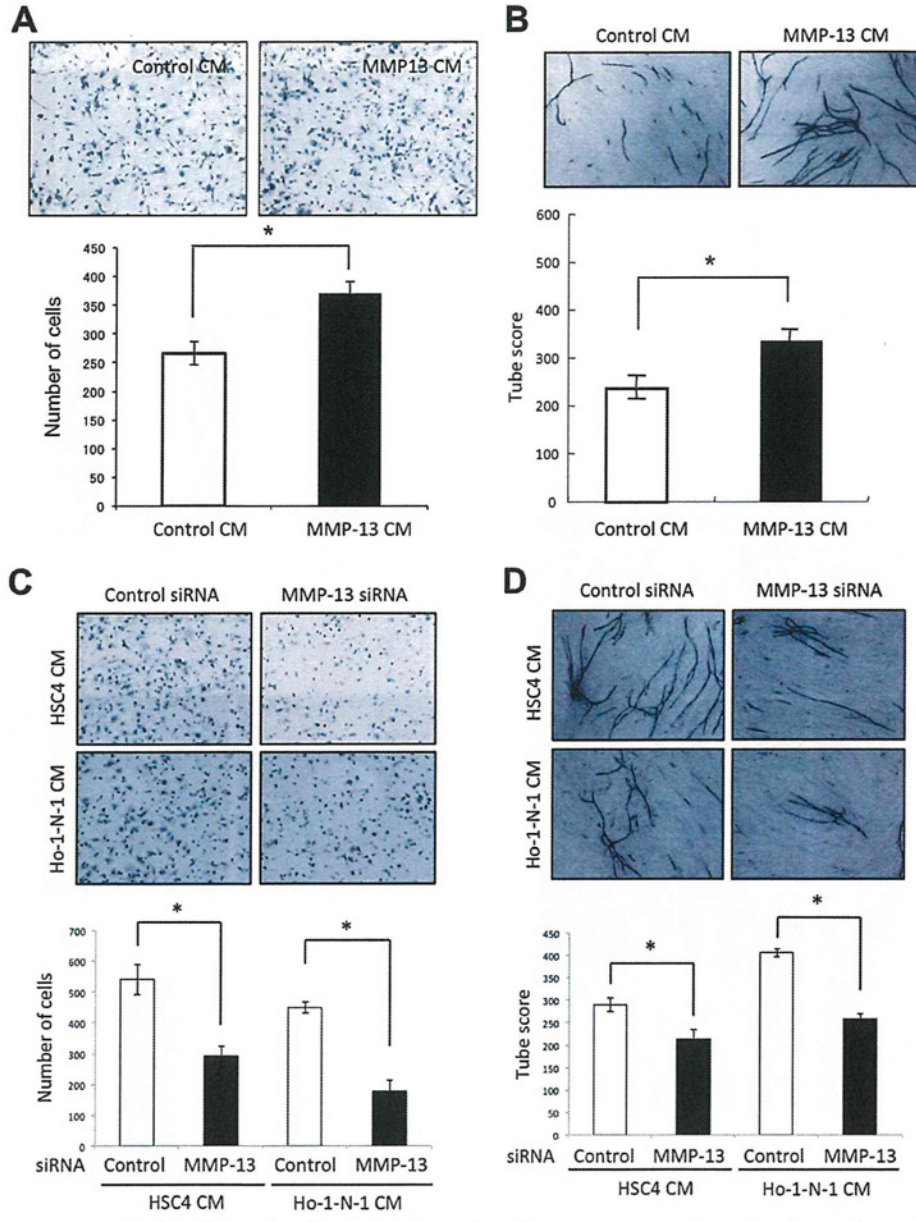

FIGURE 2. **Involvement of MMP-13 in migration and capillary tube formation of HUVECs.** *A*, migration activity by conditioned medium from MMP-13-overexpressing cells. Migration activity was measured by the use of a 24-well cell culture insert with 8-μm pores. The lower compartment contained 0.5 ml of conditioned medium from empty vector-transfected HSC3 cells (control *CM*) or MMP-13-overexpressing HSC3 cells (MMP-13 CM). After trypsinization, 5×10^4 of immortalized HUVECs (HuhT1) were resuspended in 100 μl of serum-free medium and placed in the upper compartment of the cell culture insert for 4 h. To examine the activity of migration, the cells that had penetrated onto the lower side of the filter were fixed with formalin and stained with hematoxylin. The *upper panel* shows the representative area of penetrated cells. The *lower graph* shows the average number of penetrated cells. The *bars* show the average values and S.D. of three independent experiments. *, significantly different from control at $p < 0.05$. *B*, *upper panel* shows the representative area of capillary tube formation by conditioned medium from empty vector-transfected HSC3 cells (control CM) or MMP-13-overexpressing HSC3 cells (MMP-13 CM) (×40). An angiogenesis assay kit was used according to the manufacturer's instructions with minor modifications. HUVECs were treated with mixture of conditioned medium and HuMedia-EG2 in a percentage of 1:1. The mixed media were changed every 3 days. After 12 days, the cells were fixed and stained with anti-human CD31 antibody as described under "Materials and Methods." The *lower graph* shows the average capillary tube score after conditioned medium treatment. Capillary tube score was estimated with the Chalkley count method under a bright-field microscope. The values represent means of capillary tube score + S.D. based on three wells/data point in a single experiment. *, significantly different from control at $p < 0.05$. *C*, migration activity of HuhT1 cells by conditioned medium from control or MMP-13 siRNA-treated cells. MMP-13 siRNA were transfected into HSC4 and Ho-1-N-1 cells. Migration activity was measured as described in *A*. The *upper panel* shows the representative area of penetrated cells. The *lower graph* shows the average number of penetrated cells. The *bars* show the average values and S.D. of three independent experiments. *, significantly different from control at $p < 0.05$. *D*, upper panel shows the representative area of capillary tube formation by conditioned medium from control or MMP-13-depleted cells (×40). Capillary tube formation was examined as described in *B*. The *lower graph* shows the average capillary tube score after conditioned medium treatment. Capillary tube score was estimated with the Chalkley count method under a bright-field microscope. The values represent means of capillary tube score + S.D. based on three wells/data point in a single experiment. *, significantly different from control at $p < 0.05$.